
STATE-DEPENDENT FORCES IN COLD QUANTUM GASES

Christopher Billington

Submitted in total fulfilment of the requirements
of the degree of Doctor of Philosophy

Supervisory committee:

Prof Kristian Helmerson

Dr Lincoln Turner

Dr Russell Anderson



School of Physics and Astronomy
Monash University

January, 2017

rev: 45 (b37fd8d3e6c7)
author: Chris Billington
date: Fri Mar 17 17:54:14 2017 -0400
summary: Almost completed commutation error figure.

This page intentionally left blank

Contents

| | |
|---|-----------|
| Contents | i |
| 3 Quantum mechanics on a computer | i |
| 3.1 From the abstract to the concrete: neglect, discretisation and representation | 1 |
| 3.2 Solution to the Schrödinger equation by direct exponentiation | 3 |
| 3.2.1 Matrix exponentiation by diagonalisation | 4 |
| 3.2.2 Time-ordered exponentials and time-ordered products | 5 |
| 3.2.3 The operator product/split-step method | 7 |
| 3.3 For everything else, there's fourth-order Runge–Kutta | 16 |
| 3.4 Continuous degrees of freedom | 16 |
| 3.4.1 Spatial discretisation on a uniform grid: the Fourier basis . . | 17 |
| 3.4.2 Finite differences | 21 |
| 3.4.3 The finite element discrete variable representation | 21 |
| 3.4.4 Harmonic oscillator basis functions | 22 |
| 3.5 Finding ground states | 23 |
| 3.5.1 Imaginary time evolution | 23 |
| 3.5.2 Successive over-relaxation | 23 |
| 3.5.3 Generalisation to excited states via Gram–Schmidt orthonormalisation | 23 |
| 3.6 Fourth order Runge–Kutta in an instantaneous local interaction picture | 23 |
| 3.6.1 Algorithm | 25 |
| 3.6.2 Domain of improvement over other methods | 27 |
| 3.6.3 Results | 30 |
| 3.6.4 Discussion | 32 |
| References | 35 |

rev: 45 (b37fd8d3e6c7)
author: Chris Billington
date: Fri Mar 17 17:54:14 2017 -0400
summary: Almost completed commutation error figure.

This page intentionally left blank

rev: 45 (b37fd8d3e6c7)
author: Chris Billington
date: Fri Mar 17 17:54:14 2017 -0400
summary: Almost completed commutation error figure.

Quantum mechanics on a computer

[TEXT WIDTH IS 325.0pt] This chapter comprises a summary of some of the methods used by cold atom physicists to compute numerical results pertaining to cold atom systems. Many a problem in quantum mechanics is not analytically solvable, especially when the real world of experimental physics rears its ugly head, violating theorists' assumptions of simplicity left and right. In particular, atomic physics experiments are time-dependent, with each run of an experiment generally proceeding in stages. Lasers may turn on and off, magnetic fields may vary in magnitude and direction, RF pulses may be chirped to reliably induce particular transitions [1]. Much of the numerical computation performed by researchers in cold atom physics groups such as ours are accordingly of the time-dependent variety, and are fairly literal simulations of specific experiments that may be carried out in the lab.

Here I explain some fundamentals of representing quantum mechanical problems on a computer and then present my favourite algorithms for propagating state vectors and wavefunctions in time. To spoil the surprise: my favourite timestepping algorithms are the 4th-order split-step method and (unoriginally) 4th-order Runge–Kutta, and my favourite method of evaluating spatial derivatives is moderate (6th or so) order finite differences. I think Fourier transforms for spatial derivatives are overrated, and I show that the finite element discrete variable representation (FEDVR) is, despite appearances, actually less computationally efficient than simple finite differences for producing equally accurate solutions to the spatial Schrödinger equation. I also mention some methods of finding groundstates and other stationary states, and in section 3.6 I present a modification to 4th-order Runge–Kutta that enables it to take larger timesteps for certain problems.

3.1 From the abstract to the concrete: neglect, discretisation and representation

To numerically simulate a quantum mechanical system, one must evolve a state vector in time according to the Schrödinger equation:

$$i\hbar \frac{d}{dt} |\psi(t)\rangle = \hat{H}(t) |\psi(t)\rangle. \quad (3.1)$$

To do this on a computer, one must first decide which degrees of freedom are to be simulated. We necessarily neglect many degrees of freedom as a matter of course; which ones can be neglected is warranted by the specific situation and we do it so often we barely notice. For example, simulating a single component Bose–Einstein condensate entails neglecting the internal degrees of freedom of the atoms—as well as reducing the atom–light interaction to a simple potential such as an optical dipole trap or magnetic dipole

rev: 45 (b37fd8d3e6c7)
 author: Chris Billington
 date: Fri Mar 17 17:54:14 2017 -0400
 summary: Almost completed commutation error figure.

interaction (neglecting the quantum degrees of freedom in the electromagnetic field). We may ignore one or more spatial degrees of freedom as well, say, if we are simulating an experiment in which the condensate is confined to one or two dimensions [2–4] by way of a tight trapping potential in one or more directions. Or, when simulating laser cooling [SEE SECTION ON LASER COOLING SIMS IN ATOMIC PHYSICS CHAPTER], we may care very much about the electronic state of the atom, but treat its motional state classically. In these cases we are essentially imposing the assumption that the system will only occupy one state with respect to those degrees of freedom ignored (the condensate will remain in lowest excitation level in the direction of the tight trap; the atoms will remain in one specific Zeeman sublevel), or we are assuming those degrees of freedom can be treated classically (the electromagnetic field is well described by classical electromagnetism; the atoms' motional state is described well by Newtonian mechanics). Which degrees of freedom can be neglected and which cannot requires knowledge of the situation at hand, often informed by best-practices of the research community in question and ultimately justified by experiment.¹

¹A classic example in the cold atom community of neglected degrees of freedom leading to *disagreement* with experiment is the discovery of polarisation gradient cooling (PGC), the explanation for which requires consideration of Zeeman sublevels of the atoms. The experiment that discovered PGC [5] was designed to measure the effect of Doppler cooling, which does not involve Zeeman sublevels, and it was not until afterwards that theorists determined [6] that transitions between Zeeman sublevels cannot be neglected and indeed are crucial in explaining the lower than predicted temperatures observed.

²The D-line of rubidium 87 has an energy gap of 0.6 eV, requiring a temperature of ≈ 650 K or higher in order for the Boltzmann factor $e^{-\frac{\Delta E}{k_B T}}$ describing the thermal occupation of the excited state to exceed 1×10^{-12} .

Once the degrees of freedom are known, one must decide on a basis in which to represent them concretely. The basis often cannot be complete, since for many degrees of freedom this would require an infinite number of basis states—for example the electronic state of an atom contains a countably infinite number of states, and a spatial wavefunction in free space has an uncountable number of states (one for each position in \mathbb{R}^3). For the internal state of an atom, therefore, we restrict ourselves to only the states we expect can become non-negligibly occupied, given the initial conditions and transitions involved. For example, at low temperature we can expect atoms to be almost completely in their electronic ground states, since energy gaps between ground and excited states are large compared to the thermal energy scale $k_B T$.² We need only include the small number of excited states that might become occupied as a result of optical transitions present in the situation being simulated. This can still be a large number of states if one is studying Rydberg atoms [7, 8] or using ultrafast (and therefore broad-band) laser pulses [9–11], but is otherwise fairly small. For example, including both the D1 and D2 lines of Rubidium 87, with all hyperfine levels and Zeeman sublevels gives 32 states (see section [LASER COOLING SIMS IN ATOMIC PHYSICS CHAPTER]).

For spatial degrees of freedom, we usually limit ourselves firstly to a finite region of space (we don't expect the Bose–Einstein condensate to have much probability amplitude on the Moon or anywhere else outside the vacuum system), and then we need to discretise the region of space remaining. To do this one can either discretise space on a grid, or use a set of orthogonal basis functions, and strictly speaking these can be equivalent, as we will soon see.

Once the degrees of freedom and basis vectors have been chosen, the state vector is then represented on a computer as an array of complex numbers, giving the coefficients of each basis vector required to represent a particular state vector. Matrix elements of the Hamiltonian in the same basis must be calculated, and the Schrödinger equation can then be written:

$$i\hbar \frac{d}{dt} \langle n | \psi(t) \rangle = \sum_m \langle n | \hat{H}(t) | m \rangle \langle m | \psi(t) \rangle, \quad (3.2)$$

or in standard matrix/vector notation (without Dirac notation):

$$i\hbar \frac{d}{dt} \psi_n(t) = \sum_m H_{nm}(t) \psi_m(t) \quad (3.3)$$

$$\iff i\hbar \frac{d}{dt} \psi(t) = H(t) \psi(t), \quad (3.4)$$

where $\psi_n(t) = \langle n | \psi(t) \rangle$, $H_{nm}(t) = \langle n | \hat{H}(t) | m \rangle$ and $\psi(t)$ and $H(t)$ are the vector and matrix with components and elements $\{\psi_n(t)\}$ and $\{H_{nm}\}$ respectively. This is now

something very concrete that can be typed into a computer. Programming languages generally don't know about Dirac kets and operators, and so everything that is to be computed must be translated into matrices and vectors in specific bases. This may seem so obvious as to not be worth mentioning, but was nonetheless a stumbling block in my own experience of getting to grips with quantum mechanics. Once realising that every operator has a matrix representation in some basis, at least in principle (including differential operators), and that every ket is just a list of vector components in some basis (including ones representing spatial wavefunctions), similarly at least in principle, expressions dense in bras and kets become much more concrete as the reader has a feel for exactly how they would type it into a computer. Without a good feel for the mapping between operator algebra and the actual lists of numbers that these objects imply, doing quantum mechanics on paper can seem like an exercise in abstract mumbo-jumbo.

3.2 Solution to the Schrödinger equation by direct exponentiation

As an example of something seemingly abstract being more concrete than first appearances, it is sometimes said that the 'formal' solution to the Schrödinger equation (3.1) is:

$$|\psi(t)\rangle = e^{-\frac{i}{\hbar} \int_{t_0}^t \hat{H}(t') dt'} |\psi(t_0)\rangle. \quad (3.5)$$

Saying that this is the 'formal' solution rather than just 'the solution' is presumably intended to emphasise that the arithmetic operations involved in (3.5) might not make immediate sense for the types of mathematical objects they are operating on, and that we have to be careful in defining the operations such that they produce a result that is not only sensible, but also the solution to the Schrödinger equation. If both $\hat{H}(t)$ and $|\psi(t)\rangle$ were single-valued functions of time rather than an operator valued function of time (the values at different times of which don't necessarily commute) and a vector valued function of time, then we would have no problem. However, (3.5) as written with operators and vectors is ambiguous, and we need to elaborate on it in order to ensure it is correct. I will come back to this after considering a simpler case.

If the Hamiltonian is time-independent, then (3.5) reduces to

$$|\psi(t)\rangle = e^{-\frac{i}{\hbar} \hat{H} \Delta t} |\psi(t_0)\rangle, \quad (3.6)$$

where $\Delta t = t - t_0$. Given the matrix representation H of \hat{H} and vector representation $\psi(t_0)$ of $|\psi(t_0)\rangle$ in a particular basis, this can now be directly typed into a computer as the matrix multiplication:

$$\psi(t) = U(t, t_0) \psi(t_0), \quad (3.7)$$

where

$$U(t, t_0) = e^{-\frac{i}{\hbar} H \Delta t} \quad (3.8)$$

is the (matrix representation of the) unitary evolution operator for time evolution from the initial time t_0 to time t , and is computed using a matrix exponential of $-\frac{i}{\hbar} H \Delta t$. Exponentiation of matrices is defined via the Taylor series of the exponential function:

$$e^A = \sum_{n=0}^{\infty} \frac{A^n}{n!}, \quad (3.9)$$

which reduces matrix exponentiation to the known operations of matrix multiplication and addition. However, any linear algebra programming library worth the bytes it occupies will have a matrix exponentiation function that should be used instead, as there are

other methods of computing matrix exponentials that are more computationally efficient and numerically stable, such as the Padé approximant [12]. It should be noted that there is no known ‘best’ matrix exponential algorithm, all make compromises and perform poorly for certain types of matrices [13].

3.2.1 Matrix exponentiation by diagonalisation

Regardless of which method is used, matrix exponentiation is computationally expensive. It can be sped up however if a diagonalisation of H is known, since if

$$H = QDQ^\dagger, \quad (3.10)$$

where D is a diagonal matrix and Q is a unitary matrix³, then

$$e^{-\frac{i}{\hbar}H\Delta t} = Qe^{-\frac{i}{\hbar}D\Delta t}Q^\dagger. \quad (3.11)$$

This is simple to evaluate because the exponentiation of a diagonal matrix can be performed by exponentiating each diagonal matrix element individually⁴

Even if a diagonalisation of H is not analytically known, numerically diagonalising H (using a linear algebra library function or otherwise) can form the basis for writing your own matrix exponentiation function, if needed. I found this necessary for efficiently exponentiating an array of matrices in Python, since the `scipy` and `numpy` scientific and numeric libraries at the present time lack matrix exponentiation functions that can act on arrays of matrices. Writing a `for` loop in an interpreted language such as Python to exponentiate the matrices individually in many cases is unacceptably slow, so for these cases⁵ I use a function such as the below:

³Note that the diagonals of D are the eigenvalues of H , and the columns of Q are its eigenvectors.

⁴The reason for this is clear from the Taylor series definition of matrix exponentiation, since matrix multiplication and addition can both be performed elementwise for diagonal matrices.

⁵Such as simulating the internal state of a large number of atoms, or evolving a spinor Bose–Einstein condensate by exponentiating the Zeeman Hamiltonian with a spatially varying magnetic field.

```

1 import numpy as np
2 from numpy.linalg import eig
3
4 def expm(M):
5     """Compute exp(M), where M, shape (..., N, N) is an array of N by N
6     Hermitian matrices, using the diagonalisation method. Made this function
7     because scipy's expm can't take an array of matrices as input, it can only
8     do one at a time."""
9
10    # Diagonalise the matrices:
11    evals, evecs = eig(M)
12
13    # Now we compute exp(M) = Q exp(D) Q^\dagger where Q is the matrix of
14    # eigenvectors (as columns) and D is the diagonal matrix of eigenvalues:
15
16    Q = evecs
17    Q_dagger = Q.conj().swapaxes(-1, -2) # Only transpose the matrix dimensions
18    exp_D_diags = np.exp(evals)
19
20    # Compute the 3-term matrix product Q*exp_D_diags*Q_dagger using the
21    # einsum function in order to specify which array axes of each array to
22    # sum over:
23    return np.einsum('...ik,...k,...kj->...ij', Q, exp_D_diags, Q_dagger)

```

Matrix diagonalisation (using singular value decomposition or QR decomposition) has computational time complexity $\mathcal{O}(n^3)$, where n is the number of rows/columns in the (square) matrix. Matrix multiplication is (in practice) $\mathcal{O}(n^3)$ and exponentiating a diagonal matrix is only $\mathcal{O}(n)$, so matrix exponentiation of a Hermitian matrix via numerical diagonalisation has total cost $\mathcal{O}(n^3)$. This compares to the Padé approximant, which is also $\mathcal{O}(n^3)$ [13]. So the numerical diagonalisation method is not any worse in terms of computational resources required.

On the other hand, if an analytic diagonalisation is already known, it would seem that exponentiation is just as slow, since the computational cost of matrix multiplication

alone is the same order in n as that of numerical diagonalisation. This is true—so there are only constant factors to be saved in computer time by using an analytic diagonalisation in order to exponentiate a matrix using (3.11). However if one's aim—as is often the case—is to ultimately compute

$$\psi(t) = e^{-\frac{i}{\hbar} H \Delta t} \psi(t_0), \quad (3.12)$$

for a specific $\psi(t_0)$, then one needs only matrix-vector multiplications and not matrix-matrix multiplications in order to evaluate

$$\psi(t) = U e^{-\frac{i}{\hbar} D \Delta t} U^\dagger \psi(t_0), \quad (3.13)$$

from right-to-left, reducing the computational cost to $\mathcal{O}(n^2)$ compared to evaluating it left-to-right.

Whilst matrix exponentiation is a way to efficiently evolve systems with time-independent Hamiltonians, if you only exponentiate a matrix once, you don't much care about the time complexity of doing so. It is mostly of interest because the real power of these exponentiation methods is as a building block for methods of approximate solutions to the Schrödinger equation in the case of time *dependent* Hamiltonians, as we will see in the next section.

3.2.2 Time-ordered exponentials and time-ordered products

As hinted to earlier, the solution (3.5) is not the whole picture. It can only be taken at face value if the Hamiltonian at each moment in time commutes with itself at all other times (we will see shortly why this is). If it does—that is, if $[\hat{H}(t'_1), \hat{H}(t'_2)] = 0$ for all $t'_1, t'_2 \in [t_0, t]$, then (3.5) is the solution to the Schrödinger equation, and once represented in a specific basis can be written

$$\psi(t) = U(t, t_0) \psi(t_0), \quad (3.14)$$

with

$$U(t, t_0) = e^{-\frac{i}{\hbar} \int_{t_0}^t H(t') dt'}, \quad (3.15)$$

i.e. with an integral in the exponent rather than a simple multiplication by a time interval. Since matrix addition can be performed elementwise, so can the integral in the exponent, yielding a matrix which once exponentiated will give the evolution operator $U(t, t_0)$ for the solution to the Schrödinger equation. If the Hamiltonian at each moment in time does not commute with itself at all other times, however, then the unitary evolution operator for the solution to the Schrödinger equation is instead given by the following *time-ordered exponential* [14, p. 193]:

$$U(t, t_0) = \mathcal{T} \left\{ e^{-\frac{i}{\hbar} \int_{t_0}^t H(t') dt'} \right\}. \quad (3.16)$$

In this expression, \mathcal{T} denotes the *time-ordering operator*. The time ordering operator reorders terms within products that contain a time parameter (for us, the time parameter is the argument of the matrix-valued function H), such that the value of the time parameter is smallest in the rightmost term, largest in the leftmost term, and monotonically increasing right-to-left in between. For example:

$$\mathcal{T} \{ H(4)H(1)H(2)H(5)H(3) \} = H(5)H(4)H(3)H(2)H(1). \quad (3.17)$$

We see now why the time-ordering can be neglected when $H(t)$ commutes with itself at all times. When it does, all possible reorderings of a product of copies $H(t)$ are already equal, and so a time-ordering operator leaves the actual value of the product unchanged.

Despite appearances, this time-ordered exponential is perfectly concretely defined via the definitions of all the operations involved that we have described so far, and can—with some effort—be typed into a computer and evaluated directly. Even though this is not how I have evaluated time-ordered exponentials in my simulations of atomic systems, I'll quickly elaborate on this just to emphasise the concreteness of all these operations.

“What products is T reordering?” you might ask, as (3.16) doesn't appear to contain any products of $H(t)$. On the contrary, it does, since exponentiation is defined by its Taylor series, and so

$$U(t, t_0) = 1 + T \left\{ \sum_{n=1}^{\infty} \frac{1}{n!} \left[-\frac{i}{\hbar} \int_{t_0}^t H(t') dt' \right]^n \right\} \quad (3.18)$$

$$= 1 + \sum_{n=1}^{\infty} \frac{1}{n!} \left(-\frac{i}{\hbar} \right)^n T \left\{ \left[\int_{t_0}^t H(t') dt' \right]^n \right\}. \quad (3.19)$$

Each term in this series contains the n^{th} power (and hence a product) of an integral of $H(t)$. The time ordering operator doesn't allow us to evaluate each term by computing the matrix integral once and then raising it to a power—to do so would violate time-ordering since each integral involves evaluating $H(t)$ at all times. Instead we have to write each product of integrals as the integral of a product:

$$U(t, t_0) = 1 + \sum_{n=1}^{\infty} \frac{1}{n!} \left(-\frac{i}{\hbar} \right)^n \int_{t_0}^t dt'_1 \int_{t_0}^{t'_1} dt'_2 \cdots \int_{t_0}^{t'_{n-1}} dt'_n \cdots T \{ H(t'_1) H(t'_2) \cdots H(t'_n) \}, \quad (3.20)$$

from which we can see exactly which product of matrices the time ordering operator is acting on.

Now we are close to seeing one might evaluate $U(t, t_0)$ numerically by summing each term in the Taylor series up to some order set by the required accuracy. For the n^{th} term, one needs to evaluate an n -dimensional integral over n time coordinates, with each coordinate having the same limits of integration. This can be computed in the usual way an integral is numerically computed,⁶ with the minor change that each time the integrand is evaluated, the terms within it must be re-ordered to respect the required time-ordering. Alternatively, the integration region can be restricted to the region in which the terms are already time-ordered, and then the total integral inferred by symmetry, which gives:

$$U(t, t_0) = 1 + \sum_{n=1}^{\infty} \left(-\frac{i}{\hbar} \right)^n \int_{t_0}^t dt'_n \cdots \int_{t_0}^{t'_3} dt'_2 \int_{t_0}^{t'_2} dt'_1 H(t'_n) \cdots H(t'_2) H(t'_1). \quad (3.21)$$

This is now a perfectly concrete expression, with each term comprising an integral over an n -simplex⁷ of a product of n matrices.

This expression for the unitary evolution operator is called the Dyson series [16]. It is not generally used for time-dependent simulations, though it is the basis for time-dependent perturbation theory, and sees use in high energy physics [16, 17] for computing transition amplitudes between incoming and outgoing waves in scattering problems (in which U is called the S -matrix). In these problems, H is an interaction Hamiltonian containing terms for all particle interactions being considered. Accordingly, the integrand for the n^{th} term, being a product of n copies of H evaluated at different times, contains one term for each possible sequence of particle interactions. The integral itself can be considered a sum of transition amplitudes over all possible times that each interaction could have occurred. Indeed, each term in the Dyson series corresponds to a number of Feynman diagrams with n nodes [17].

⁶By sampling the integrand on a uniform grid, using a quadrature method, or Monte-Carlo integration [15] which is widely used for high dimensional integrals such as these.

⁷A simplex is the generalisation of a triangle to higher dimensions, i.e. a 3-simplex is a tetrahedron.

The Dyson series isn't really suited to time-dependent simulations, though perturbation theory is useful for approximate analytics. For one, the series must be truncated at some point, and the result won't be a U that is actually unitary.⁸ Also, we are typically interested in the intermediate states, not just the final state of a system or an average transition rate, as one might want to compute in a scattering problem.

In any case, usually when solving the Schrödinger equation by exponentiation we use the following, alternate expression for a time-ordered exponential:

$$U(t, t_0) = T \left\{ e^{-\frac{i}{\hbar} \int_{t_0}^t H(t') dt'} \right\} \quad (3.22)$$

$$= \lim_{N \rightarrow \infty} \prod_{n=N-1}^0 e^{-\frac{i}{\hbar} H(t_n) \Delta t}, \quad (3.23)$$

where here $\Delta t = (t - t_0)/N$ and $t_n = t_0 + n\Delta t$. Note that the product limits are written in the reverse of the usual order—this is important in order to produce terms with smaller n on the right and larger n on the left of the resulting product. You can convince yourself that (3.21) is equivalent to (3.23) this by replacing the integral in the exponent with a sum—as per the Riemann definition of an integral—and expanding the exponential according to its Taylor series. Expanding each exponential in (3.23) as a Taylor Series and collecting terms of equal powers of H then reveals that the two Taylor series are identical.

In any case, (3.23) paints an intuitive picture of solving the Schrödinger equation: one evolves the initial state vector in time by evolving it according to constant Hamiltonians repeatedly over small time intervals⁹. This has the desirable property that all intermediate state vectors are computed at the intermediate steps, meaning one can study the dynamics of the system and not just obtain the final state. This is of course useful for comparison with experiments, plenty of which involve time-dependent data acquisition and not just post-mortem analysis of some evolution.

Numerically, we can't actually take $N \rightarrow \infty$, or equivalently $\Delta t \rightarrow 0$, and so we instead choose a Δt smaller than the timescale of any time-dependence of H , and step through time using

$$\psi(t_{n+1}) = e^{-\frac{i}{\hbar} H(t_n) \Delta t} \psi(t_n) + \mathcal{O}(\Delta t^2) \quad (3.24)$$

$$\Rightarrow \psi(t) = \left(\prod_{n=N-1}^0 e^{-\frac{i}{\hbar} H(t_n) \Delta t} \right) \psi(t_0) + \mathcal{O}(\Delta t). \quad (3.25)$$

Thus the case of a time-dependent Hamiltonian reduces to repeated application of the solution (3.7) for a time-independent Hamiltonian, and is (globally) accurate to order Δt . Note that the entire expression can be evaluated right-to-left to propagate the initial state vector in time without explicitly computing the overall unitary, which ensures the computational complexity is $\mathcal{O}(n^2)$ in the size of the system (when the exponentiation is performed via an analytic or pre-computed diagonalisation) rather than $\mathcal{O}(n^3)$.

3.2.3 The operator product/split-step method

Here I'll review decompositions similar to (3.24), but which use variable timesteps to achieve an accuracy to higher order in Δt . I'll present them at the same time as addressing another problem, which is that Hamiltonians are often not in a simple enough form to be exponentiated efficiently at all, making (3.24) difficult to evaluate. Often Hamiltonians are a sum of non-commuting operators (such as kinetic and potential terms), with time dependence such that any diagonalisation of the overall Hamiltonian at one point in time will not diagonalise it at another point in time, with the system size large

⁸Although unitarity is not often a strict requirement - we also frequently solve (3.3) directly with fourth order Runge-Kutta, which is also not unitary.

⁹This is the usual definition of the solution to a differential equation, which is why I prefer to think of the product formula (3.23) as the *definition* of the solution to the Schrödinger equation, and the time-ordered exponential as merely a shorthand notation for it.

enough for numerical diagonalisation to be prohibitively expensive. In these cases, we can use methods called *split-step* or *operator product* methods, which allow one to approximately exponentiate the entire Hamiltonian based on having exact diagonalisations of its component terms. In the case of time-dependent Hamiltonians, this allows us to avoid rediagonalising at every timestep whenever the time-dependence can be expressed as scalar coefficients multiplying time-independent operators:

$$\hat{H}(t) = \alpha(t)\hat{H}_1 + \beta(t)\hat{H}_2 + \dots, \quad (3.26)$$

since multiplication of a matrix by a scalar merely scales its eigenvalues, leaving its eigenbasis unchanged.

There is little downside to having an only approximate exponentiation of the Hamiltonian when the timestepping is already only approximate, so long as we ensure that neither source of error is much greater than the other. To this end I'll show split-step methods that have (global) error $\mathcal{O}(\Delta t)$, $\mathcal{O}(\Delta t^2)$ and $\mathcal{O}(\Delta t^4)$. In section 3.4, we'll see how this method applies to the case of a spatial wavefunction obeying the Gross–Pitaevskii equation.

First order split-step

Say we have (the matrix representation of) a Hamiltonian that is the sum of two non-commuting terms:¹⁰

$$H(t) = H_1(t) + H_2(t). \quad (3.27)$$

The unitary for the solution to the Schrödinger equation is as before:

$$U(t, t_0) = \mathcal{T} \left\{ e^{-\frac{i}{\hbar} \int_{t_0}^t H(t') dt'} \right\}, \quad (3.28)$$

which, without loss of exactness, we can split into N equal time intervals of size Δt and write

$$U(t, t_0) = \prod_{n=N-1}^0 U(t_{n+1}, t_n), \quad (3.29)$$

where again $t_n = t_0 + n\Delta t$ and $\Delta t = (t - t_0)/N$, and where

$$U(t_{n+1}, t_n) = \mathcal{T} \left\{ e^{-\frac{i}{\hbar} \int_{t_n}^{t_{n+1}} H(t') dt'} \right\}. \quad (3.30)$$

Evaluating the integral using a one-point rectangle rule gives

$$U(t_{n+1}, t_n) = e^{-\frac{i}{\hbar} H(t_n)\Delta t + \mathcal{O}(\Delta t^2)}, \quad (3.31)$$

in which we were able to drop the time ordering operator because $H(t)$ is only evaluated at a single time. Using the Taylor series definition of the exponential, we can take the error term out of the exponent and write

$$U(t_{n+1}, t_n) = e^{-\frac{i}{\hbar} H(t_n)\Delta t} + \mathcal{O}(\Delta t^2). \quad (3.32)$$

So far all we've done is justify (3.24). Now we'll acknowledge that H is a sum of two terms and write:

$$U(t_{n+1}, t_n) = e^{-\frac{i}{\hbar} (H_1(t_n) + H_2(t_n))\Delta t} + \mathcal{O}(\Delta t^2). \quad (3.33)$$

¹⁰From here on, component terms of the Hamiltonian will be written with general time dependence, even though it is understood that these methods are mostly useful for the case where that time dependence can be written as scalar coefficients multiplying otherwise time-independent matrices.

Using the Baker–Campbell–Hausdorff formula [14, p. 158], we can expand the exponential as:

$$e^{-\frac{i}{\hbar}(H_1(t_n)+H_2(t_n))\Delta t} = e^{-\frac{i}{\hbar}H_1(t_n)\Delta t} e^{-\frac{i}{\hbar}H_2(t_n)\Delta t} e^{\frac{1}{2\hbar^2}[H_1(t_n),H_2(t_n)]\Delta t^2 + \mathcal{O}(\Delta t^3)} \quad (3.34)$$

$$\Rightarrow U(t_{n+1}, t_n) = e^{-\frac{i}{\hbar}H_1(t_n)\Delta t} e^{-\frac{i}{\hbar}H_2(t_n)\Delta t} + \mathcal{O}(\Delta t^2). \quad (3.35)$$

So we see that the ‘commutation error’ in (3.35) caused by treating the two terms as if they commute is of the same order in Δt as the ‘integration error’ in (3.32) caused by treating the overall Hamiltonian as time-independent over one timestep, resulting in a method with local error $\mathcal{O}(\Delta t^2)$ and global error $\mathcal{O}(\Delta t)$; the first order split-step method:

$$U(t, t_0) = \prod_{n=N-1}^0 U_1(t_{n+1}, t_n) + \mathcal{O}(\Delta t), \quad (3.36)$$

where

$$U_1(t_{n+1}, t_n) = e^{-\frac{i}{\hbar}H_1(t_n)\Delta t} e^{-\frac{i}{\hbar}H_2(t_n)\Delta t}. \quad (3.37)$$

Using the diagonalisation method of matrix exponentiation discussed in section 3.2.1, this unitary U_1 can be used to step a state vector through time with only matrix-vector multiplications and scalar exponentiation, where separate diagonalisations of H_1 and H_2 are either analytically known or pre-computed, even though a diagonalisation of the total Hamiltonian H may not be feasible.

Crucially, if H_1 and H_2 act on different subspaces of the overall Hilbert space, with respective dimensionalities n_1 and n_2 , that is, $H_1(t) = \tilde{H}_1(t) \otimes \mathbb{I}_{n_2}$ and $H_2(t) = \mathbb{I}_{n_1} \otimes \tilde{H}_2(t)$, where \mathbb{I}_m is the $m \times m$ identity matrix, then the matrix-vector products involved in applying U_1 to a state vector can be much faster ($\mathcal{O}(n_1^2 n_2 + n_1 n_2^2)$ rather than $\mathcal{O}(n_1^2 n_2^2)$) than if the Hamiltonian weren’t split into two terms, even if an analytic diagonalisation of the total Hamiltonian were available:

$$U_1(t_{n+1}, t_n) = \left(e^{-\frac{i}{\hbar}\tilde{H}_1(t_n)\Delta t} \otimes \mathbb{I}_{n_2} \right) \left(\mathbb{I}_{n_1} \otimes e^{-\frac{i}{\hbar}\tilde{H}_2(t_n)\Delta t} \right). \quad (3.38)$$

By applying (3.35) recursively for the case where either H_1 or H_2 is itself the sum of two further terms, (3.37) immediately generalises to the case where H is a sum of an arbitrary number of non-commuting terms:

$$U_1(t_{n+1}, t_n) = \prod_{m=1}^M e^{-\frac{i}{\hbar}H_m(t_n)\Delta t}, \quad (3.39)$$

where $H(t) = \sum_{m=1}^M H_m(t)$.

Second and fourth order split-step

By using a two-point trapezoid rule for the integral in (3.30), evaluating $H(t)$ at the beginning and end of the timestep, one can instead obtain an integration error of $\mathcal{O}(\Delta t^3)$ per step:

$$U(t_{n+1}, t_n) = e^{-\frac{i}{\hbar}(H(t_n)+H(t_{n+1}))\frac{\Delta t}{2}} + \mathcal{O}(\Delta t^3) \quad (3.40)$$

$$= e^{-\frac{i}{\hbar}(H_1(t_n)+H_2(t_n)+H_1(t_{n+1})+H_2(t_{n+1}))\frac{\Delta t}{2}} + \mathcal{O}(\Delta t^3). \quad (3.41)$$

Then, applying the Baker–Campbell–Hausdorff formula once more, and replacing $H_1(t_{n+1})$ (and similarly for $H_2(t_{n+1})$) wherever it appears in a commutator with the Taylor series

$H_1(t_n) + \dot{H}_1(t_n)\Delta t + \mathcal{O}(\Delta t^2)$, one can show that if the individual exponentials are ordered in the following way, then the remaining commutation error is also $\mathcal{O}(\Delta t^3)$:

$$U(t_{n+1}, t_n) = e^{-\frac{i}{\hbar}H_2(t_{n+1})\frac{\Delta t}{2}} e^{-\frac{i}{\hbar}H_1(t_{n+1})\frac{\Delta t}{2}} e^{-\frac{i}{\hbar}H_1(t_n)\frac{\Delta t}{2}} e^{-\frac{i}{\hbar}H_2(t_n)\frac{\Delta t}{2}} + \mathcal{O}(\Delta t^3). \quad (3.42)$$

This gives the second order split-step method:

$$U(t, t_0) = \prod_{n=N-1}^0 U_2(t_{n+1}, t_n) + \mathcal{O}(\Delta t^2), \quad (3.43)$$

where

$$U_2(t_{n+1}, t_n) = e^{-\frac{i}{\hbar}H_2(t_{n+1})\frac{\Delta t}{2}} e^{-\frac{i}{\hbar}H_1(t_{n+1})\frac{\Delta t}{2}} e^{-\frac{i}{\hbar}H_1(t_n)\frac{\Delta t}{2}} e^{-\frac{i}{\hbar}H_2(t_n)\frac{\Delta t}{2}}, \quad (3.44)$$

or, for an arbitrary number of terms in the Hamiltonian,

$$U_2(t_{n+1}, t_n) = \left(\prod_{m=M}^1 e^{-\frac{i}{\hbar}H_m(t_{n+1})\frac{\Delta t}{2}} \right) \left(\prod_{m=1}^M e^{-\frac{i}{\hbar}H_m(t_n)\frac{\Delta t}{2}} \right). \quad (3.45)$$

U_2 can be concisely written in terms of U_1 as:

$$U_2(t_{n+1}, t_n) = U_1^\dagger(t_n + \frac{\Delta t}{2}, t_{n+1}) U_1(t_n + \frac{\Delta t}{2}, t_n), \quad (3.46)$$

which is to say it is simply two applications of U_1 , each of duration half a total timestep, and with the multiplication order of the exponentials reversed in one compared to the other. Two shortcuts are immediately apparent when computing U_2 or its action on a vector: firstly, if there is a time-independent term in the Hamiltonian, it should be assigned to H_1 , so that the innermost two exponentials in (3.44) can be collapsed into one; secondly the final exponential of each timestep is identical to the first exponential of the next timestep, and so these can also be collapsed together (being split apart only at points in time when one wishes to sample the state vector).

The fourth order split-step method is much more difficult to derive, with a large number of commutators needing to cancel exactly to ensure the local error cancels out up to fourth order in Δt . It can be stated in terms of the second order split-step method as [18, p7; 19, 20]:

$$U(t, t_0) = \prod_{n=N-1}^0 U_4(t_{n+1}, t_n) + \mathcal{O}(\Delta t^4), \quad (3.47)$$

where

$$\begin{aligned} U_4(t_{n+1}, t_n) = & U_2(t_{n+1}, t_{n+1} - p\Delta t) \\ & \times U_2(t_{n+1} - p\Delta t, t_{n+1} - 2p\Delta t) \\ & \times U_2(t_{n+1} - 2p\Delta t, t_n + 2p\Delta t) \\ & \times U_2(t_n + 2p\Delta t, t_n + p\Delta t) \\ & \times U_2(t_n + p\Delta t, t_n), \end{aligned} \quad (3.48)$$

where $p = 1/(4 - 4^{1/3})$. U_4 comprises five applications of U_2 with timesteps $p\Delta t$, $p\Delta t$, $(1 - 4p)\Delta t$, $p\Delta t$, and $p\Delta t$ respectively. The innermost timestep is backwards in time, since $(1 - 4p) < 0$. But this is no problem, one simply evaluates the expression for U_2 with a negative timestep exactly as written, so long as one reads Δt when written within the above expressions for $U_1(t_f, t_i)$ and $U_2(t_f, t_i)$ as referring to $t_f - t_i$, i.e. the difference between the two arguments to the expression, not its absolute value, and not to the timestep of the method in which it is embedded.

rev: 45 (b37fd8d3e6c7)
author: Chris Billington
date: Fri Mar 17 17:54:14 2017 -0400
summary: Almost completed commutation error figure.

Parallelisability and other speedups for banded matrices

Expressions such as (3.44) don't at first glance appear particularly easy to parallelise, that is, to be evaluated in such a way as to leverage the computing power of multiple CPU cores, GPU cores, or multiple computers. A series of Hamiltonian terms must be exponentiated one by one and multiplied together. Whilst each exponential factor could be evaluated independently, and then all of them multiplied together before being applied to a state vector, this explicit construction of U is very costly compared to merely computing its action on a particular state vector, since the latter allows each term to act only in its specific subspace of the overall Hilbert space, and avoids having to pay the $\mathcal{O}(n^3)$ cost of matrix-matrix multiplication.

When one or more terms in the Hamiltonian has a matrix representation which is banded however, that is, all its entries further than a finite number of elements away from the main diagonal are zero, then those terms may be written as a sum of block diagonal matrices, for example:

[illegible]

where zero-valued matrix elements outside the band are omitted, and those within the band replaced with dots. In this example, we first take the original 16×16 matrix A , and create four 4×4 nonoverlapping submatrices whose diagonals lie along A 's main diagonal. These submatrices don't quite cover all of A 's nonzero elements, however, so we expand each submatrix (except the final one) from its bottom-right by two elements, making it a 6×6 matrix. The submatrices are no longer non-overlapping, so we take every second one and put it in a matrix B , every other one and put it in a matrix C such that B and C are both block diagonal, divide the elements they have in common by two so we don't double count them, and then declare that $A = B + C$. In the general case, the amount of overlap between the submatrices required to encompass all of A is equal to the bandwidth b of A (in this case $b = 2$ since A has two non-main diagonals on each side of its main diagonal).

Having split a term in the Hamiltonian into two terms, we can simply apply the split operator method as normal, with the same order accuracy in Δt as before. But now the matrices that we wish to exponentiate and have act on a vector are *block diagonal*. This means that the exponentiation of each block can be applied (using the diagonalisation

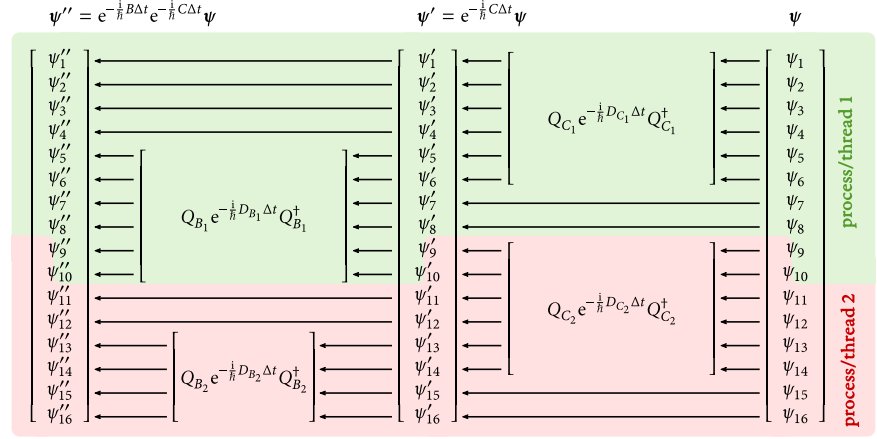


Figure 3.1: Schematic of data flow for parallel split-step method. Computation proceeds right to left. To compute the action of $e^{-\frac{i}{\hbar} B \Delta t} e^{-\frac{i}{\hbar} C \Delta t}$ on a vector ψ , one can treat the submatrices B_1 , B_2 , C_1 and C_2 , of the block-diagonal matrices B and C separately. First, the exponentiation of C can be applied to ψ by applying the exponentiations of C_1 and C_2 to ψ . If diagonalisations $C_1 = Q_{C_1} D_{C_1} Q_{C_1}^\dagger$ and $C_2 = Q_{C_2} D_{C_2} Q_{C_2}^\dagger$ are known, then the two operations can be applied as a series of matrix-vector multiplications and the exponentiation of diagonal matrices. Because the two submatrices are non-overlapping, they can be applied to the vector completely independently in separate computer processes, CPU or GPU threads, or cluster nodes. The exponentiation of B can then be applied to the resulting intermediate vector ψ' , similarly via two independent operations acting on nonoverlapping elements of ψ' . However, because each submatrix of C overlaps each submatrix of B by $b = 2$ elements on either side (b being the bandwidth of the original matrix $A = B + C$), threads/processes must share these elements (here the ninth and tenth elements), sending them to each other whenever they have been updated.

method) separately to the vector, independently of each other block. This enables the application of the exponentials to be performed in parallel—each block submatrix modifies different elements of the vector. So one might store different parts of the state vector on different nodes on a cluster computer, and compute $e^{-\frac{i}{\hbar} C \Delta t} \psi$ in parallel. Then some data exchange between nodes would be necessary before applying $e^{-\frac{i}{\hbar} B \Delta t}$ to the result (See Figure 3.1 for a schematic of how this works).

Whilst this specific banded matrix A is small for the sake of example, in general of course one might have a matrix of any size, allowing for B and C to contain more than two submatrices each. The submatrices have a minimum size of twice the bandwidth b of A , in order to cover all elements of A whilst only sharing elements with their nearest neighbour submatrices (any smaller and they would share elements with their next nearest neighbour submatrices as well, complicating things somewhat). But the only maximum is the size of A itself. So what is the optimal submatrix size? Although the split-step method is still accurate to the same order in Δt no matter how many pieces we split a banded matrix into, we clearly introduce additional ‘commutation error’ every time we split A into additional submatrices. So one might think that the number of pieces ought to be minimised, and hence the submatrix size maximised. With regard to this, one might decide to split A into $2n_{\text{threads}}$ submatrices (where n_{threads} is the number of independent computational threads available), half of which will reside in B and half in C . This minimises the extra commutation error subject to the constraint that all threads are put to use—splitting A into yet smaller pieces within one computational thread will only yield unnecessary additional error.

Is this the best option? No. Despite the extra commutation error, there is additional benefit to splitting A into more submatrices than required for parallelisation. Let s be the

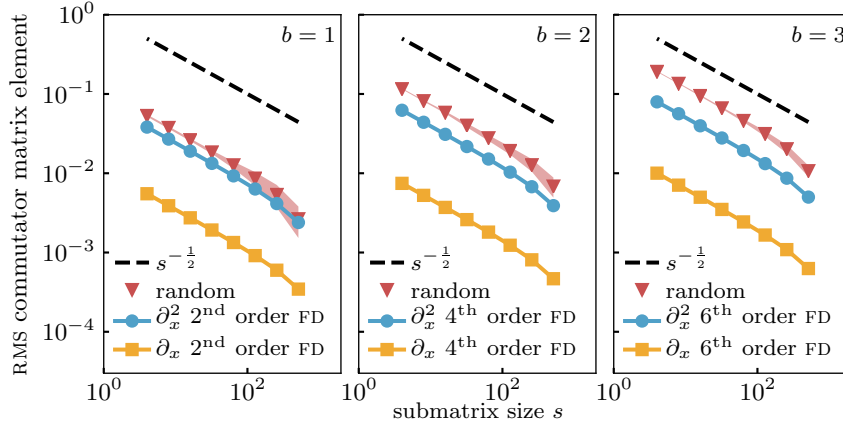


Figure 3.2: Numerical experiment to determine how the commutation error scales with the submatrix size when splitting certain banded matrices into the sum of block-diagonal matrices and using a split-operator method to exponentiate the sum. From left to right, matrices with bandwidth $b = 1$, $b = 1$ and $b = 2$ are considered. For each bandwidth, the matrices for the finite difference schemes of the order resulting in that bandwidth for first and second derivatives are considered, as well as random matrices of the given bandwidth. The random matrices have their real and imaginary parts of their nonzero elements drawn from standard normal distributions. All matrices are 1024×1024 . Calculations with random matrices were performed on 20 independent random matrices, and the mean and standard deviation (shaded) of the results plotted. The error metric is the RMS element of the commutator $[B, C]$, where the original matrix A is split into the sum of block-diagonal matrices $B + C$ using a submatrix size of s (described in-text). The RMS error in a vector propagated with the split-operator method is proportional this error metric. The result in all cases is that the commutator error, and therefore the error in the split-operator method scales with the submatrix size as $s^{-\frac{1}{2}}$.

‘nominal’ size of each submatrix, that is, the size of the corresponding *non-overlapping* submatrices prior to expanding each one along the diagonal (creating overlap) by a number of elements equal to the bandwidth b . The computational cost of the matrix-vector multiplications for computing the action of $e^{-\frac{i}{\hbar} B \Delta t} e^{-\frac{i}{\hbar} C \Delta t}$ on a vector is then $\mathcal{O}((s+b)^2)$ per submatrix, since $s+b$ is the size of the submatrices in terms of their nominal size and the bandwidth. The total number of submatrices required to cover A is ns^{-1} , where n is the size of A , and so the total cost of applying the exponentiations of all submatrices to a vector is $\mathcal{O}(ns^{-1}(s+b)^2)$. The cost *per unit time* of simulation is then $\mathcal{O}(n\Delta t^{-1}s^{-1}(s+b)^2)$. Here we see that splitting into smaller submatrices is desirable from the point of view of speed: because matrix-vector multiplication runs in quadratic time, a larger number of smaller matrices can be multiplied by vectors faster than a smaller number of larger matrices.

But the more submatrices, the more commutation error. Extra error can be made up for by making the timestep smaller, which increases the cost per unit time once more. So is it worth it? The extra commutation error from splitting up A into more and more pieces in general depends on the form of A . I performed a small numerical experiment to see how the commutator $[B, C]$ (which the commutation error is proportional to) scales with s for random banded matrices, as well as those corresponding to 2nd, 4th and 6th order finite differences for first and second derivatives. The result in all cases was that the commutator scaled as $s^{-\frac{1}{2}}$ (see Figure 3.2).

Back to our question—does decreasing the timestep size Δt to compensate for the additional commutation error result in more, or less computational cost per unit time than if we hadn’t split A into more pieces than required for parallelisation? Taking into

subspaces with dimensionalities $\{n_i\}$ is the dimensionality of the total Hilbert space, and $\{b_i\}$ are the bandwidths of the matrix representations of each term in the Hamiltonian in the chosen basis.¹¹ Furthermore, the method is efficiently parallelisable, provided the maximum size-to-bandwidth ratio $\max_i(n_i/b_i)$ of the terms in the Hamiltonian is much larger than the number of parallel computing threads available. Although the constant factors that big-O notation neglects may not be optimal, this scaling would seem to be the best one could hope for—for each of the N elements in the state vector one must consider the $\sum_i b_i$ elements (including itself) that the Hamiltonian couples it with, and no more.¹²

The main downside of this otherwise excellent method of exponentiating Hamiltonians is that the evolution modelled must actually be described by a linear system of equations. One cannot add arbitrary terms and nonlinear operators to the Hamiltonian, as the split-step method requires that one can evaluate each time-dependent term in the Hamiltonian at specific times, including times at which the solution for the state vector is not yet available. This would seem to limit the split-step method strictly to modelling *linear* dynamics, that is, terms in the Hamiltonian must not depend explicitly on the state vector they are operating on. Whilst nature might fundamentally be described by linear dynamics, once approximations of various kinds are made in order to make problems tractable, it's extremely common to end up with a nonlinear pseudopotential or nonlinear effective Hamiltonian. Note that non-*Hermitian*, pseudo-Hamiltonians—leading to non-unitary evolution—are fine. The split-step method has made no assumptions that rules them out, it only assumes the differential equation can be expressed in the form

$$\frac{d}{dt}\psi(t) = \sum_n H_n(t)\psi(t), \quad (3.52)$$

where $\{H_n\}$ are a set of linear operators, Hermitian or not.

Fortunately, one specific form of nonlinearity that cold atom physicists are particularly interested in—the nonlinear term in the Gross–Pitaevskii equation—can be incorporated without much difficulty. As mentioned, the problem with nonlinearity is that all but the first-order split step methods require you to evaluate terms in the Hamiltonian at some future time at which the state vector is not yet known, that is the algorithm contains steps akin to $\psi(t_{n+1}) = U(t_{n+1}, t_n; \psi(t_{n+1}))\psi(t_n)$ for some nonlinear unitary matrix $U(t_{n+1}, t_n; \psi(t_{n+1}))$ — U cannot be explicitly constructed because it both requires and is required by $\psi(t_{n+1})$.

For the Gross–Pitaevskii effective Hamiltonian, the second-order split-step method (from which the fourth order method is constructed) for a single step might be naïvely written

$$\psi(t_{n+1}) = e^{-\frac{i}{\hbar}K\frac{\Delta t}{2}} e^{-\frac{i}{\hbar}(g\rho(t_{n+1})+V(t_{n+1}))\frac{\Delta t}{2}} e^{-\frac{i}{\hbar}(g\rho(t_n)+V(t_n))\frac{\Delta t}{2}} e^{-\frac{i}{\hbar}K\frac{\Delta t}{2}} \psi(t_n), \quad (3.53)$$

where $\psi(t)$ is the state vector¹³ represented in a discrete position basis, g is the nonlinear interaction constant, $V(t)$ and $\rho(t) = \psi(t)\psi^\dagger(t)$ are diagonal matrices for the external potential and the density matrix for $\psi(t)$ in the same position basis, and K is a discrete approximation to the kinetic energy operator in the position basis.

As written, this can't be evaluated because $\psi(t_{n+1})$ —required to evaluate $\rho(t_{n+1})$ —is not yet known. The order we choose to exponentiate the terms in our Hamiltonian is arbitrary, however (so long as we alternately reverse that order each half-step as required by the second order split-step method), and so swapping the order gives

$$\psi(t_{n+1}) = e^{-\frac{i}{\hbar}(g\rho(t_{n+1})+V(t_{n+1}))\frac{\Delta t}{2}} e^{-\frac{i}{\hbar}K\Delta t} e^{-\frac{i}{\hbar}(g\rho(t_n)+V(t_n))\frac{\Delta t}{2}} \psi(t_n), \quad (3.54)$$

which incidentally has the benefit that since K is (ordinarily) time independent, the two adjacent exponentials containing it can be combined into one. Now $\rho(t_{n+1})$ is contained

¹¹Now that we are here, we can finally say something about the best basis for simulating in: to minimise computational costs, the best basis is the one that minimises precisely this sum of bandwidths. The exception to this is when fast Fourier transforms are involved, which I discuss later.

¹²Assuming the banded matrices are otherwise dense within their band—further improvements would be possible if some elements within the band were always zero.

¹³Usually when modelling the GPE the single-particle state vector is normalised to the number of particles, rather than unity, and so strictly speaking it cannot be called a state vector, though it otherwise can be treated as one in most respects.

within the leftmost exponential, and so it is the last operator to be applied in the timestep. Note that since $g\rho(t)$ is real and diagonal in the position basis (as is $V(t)$), this leftmost unitary merely changes the phase of the state vector at each point in space, having no effect on its density. This means that $\rho(t)$ is, in fact, unaffected by this last unitary evolution operator. Hence, $\rho(t_{n+1})$ can be computed simply as the density matrix of the intermediate state vector that this unitary was to act on:

$$\rho(t_{n+1}) = \psi(t_{n+1})\psi^\dagger(t_{n+1}) = \tilde{\psi}\tilde{\psi}^\dagger, \quad (3.55)$$

where

$$\tilde{\psi} = e^{-\frac{i}{\hbar}K\Delta t} e^{-\frac{i}{\hbar}(g\rho(t_n)+V(t_n))\frac{\Delta t}{2}} \psi(t_n). \quad (3.56)$$

The inclusion of $V(t)$ with $g\rho(t)$ is optional, and if $V(t)$ was not real valued, would not be valid (since in that case the density *would* be affected by the evolution induced by $V(t)$). In such a case the Hamiltonian would have to be split into three terms with $V(t)$ and $g\rho(t)$ treated separately.

So now we can put some conditions on what types of nonlinear operators can be used within the second-order split step method. The first condition is that at most one nonlinear operator can be included, since it must be placed last in the sandwich of exponentials (otherwise its value at the end of the timestep cannot be inferred immediately prior to acting on the state vector). The second condition is that the nonlinear operator must be invariant with respect to the evolution that it itself induces in the state vector. Here we have an operator that depends only on the state vector's absolute value, but for which the corresponding unitary only evolves the state vector's phase. Another example might be an operator that depends only on the state vector's phase gradients, but evolves the state vector's absolute value, and so forth.

Although I find this argument compelling for second-order split-step, it's less obvious that it should hold for fourth-order split-step as well, which, even though it is based on multiple applications of second-order split-step, involves a substep that is backwards in time. 'Evaluate the nonlinear operator based on the state vector at this specific time' becomes ambiguous when that moment in time is traversed in both directions by two different sub-steps. However, [22] have verified using computer symbolic algebra that indeed, up to even higher order split-step methods, putting the nonlinear density term last in the splitting and always evaluating it using the value of the intermediate state vector immediately prior results in the method having the same order accuracy in Δt as for linear operators only. Given this and my argument above, as well as the reasoning that the second-order split-step method has no way of 'knowing' whether it is acting backward in time or not when embedded in a higher-order split step method, I would expect the same to hold for all nonlinear operators meeting the above two conditions, though I haven't shown this explicitly.

3.3 For everything else, there's fourth-order Runge–Kutta

[summarise and say why it's more general. Biggest downside is error isn't bounded, other downside related to what the RK4ILIP section tries to improve]

3.4 Continuous degrees of freedom

The single-particle, non-relativistic, scalar Schrödinger wave equation, as distinct from the general Schrödinger equation [EQREF], is:

[EQUATION].

As mentioned in [SECREf], the equation for the single-particle wavefunction of an atom in a single-component Bose–Einstein condensate is the Gross–Pitaevskii equation

rev: 45 (b37fd8d3e6c7)
author: Chris Billington
date: Fri Mar 17 17:54:14 2017 -0400
summary: Almost completed commutation error figure.

[EQUATION],

where $\psi(\mathbf{r}) = \sqrt{N} \langle \mathbf{r} | \psi \rangle$ is the single-particle wavefunction scaled by the square root number of atoms N .

Both these equations are partial differential equations involving both spatial and temporal derivatives. But in quantum mechanics all state vectors can be mapped to column vectors and all operators to matrices. Spatial wavefunctions are no exception to the former and differential operators such as ∇^2 are no exception to the latter. So what do these vectors and operators look like? That depends on whether we choose to discretise space on a grid, or use a functional basis (and on which functional basis we choose). As we'll see below, however, spatial discretisation is actually just a particular choice of functional basis, namely the Fourier basis.

3.4.1 Spatial discretisation on a uniform grid: the Fourier basis

[This section incomplete: TODO: Simplify all the algebra by giving everything a single index instead of 2 indices for the 2D examples - it's too confusing with two indices on everything. Distinguish discrete vs continuous eigenkets with a different symbol - maybe a tilde over the \mathbf{r} or something like that]

Imagine a two dimensional spatial region within which we are solving the single-component Gross–Pitaevskii equation, evolving an initial condensate wavefunction in time. Having specified which degrees of freedom we want to simulate (two continuous degrees of freedom, one for each spatial dimension), the next step according to the method outlined in [SECREP ABOVE] is to choose a basis in which to represent this state vector.

Lets say we discretise space in an equally-spaced $N_x \times N_y = 5 \times 5$ rectangular grid,¹⁴ with spacing Δx , and only represent the wavefunction at those 25 points in space. The state vector can then be represented by a list of 25 complex numbers, each taken to be the wavefunction's value at the spatial position corresponding to one gridpoint. This 25-vector is now a concrete representation of our state vector.

[FIGURE SHOWING UNWRAPPING OF 2D REGION INTO COLUMN VECTOR. PERHAPS 2D REGION IS CONTINUOUS WITH A GRID SUPERIMPOSED ON IT, AND LINES JOIN EACH GRIDPOINT TO THE VECTOR AT RIGHT]

But at what point did we choose a basis just now—what are the basis vectors? This just looks like discretising space at a certain resolution, rather than the formal process of choosing a basis and projecting the state vector and operators onto each basis vector, as outlined in [SECREP ABOVE]. Assuming what we've done is equivalent to choosing a basis, that basis has a finite number (25) of basis vectors, which means it cannot be complete, since state vectors we're approximately representing with it require an infinite number of complex numbers to be described exactly.¹⁵ So what do the basis functions look like, and what state vectors have we implicitly excluded from simulation by choosing a basis that is incomplete?

As a sidenote, spatial wavefunctions are often described as the representation of wavefunctions in the “spatial basis”—a basis in which the basis vectors $\{|\mathbf{r}\rangle\}$ are Dirac-deltas centred on each point in space [CITE DIRAC'S BOOK MAYBE]. The wavefunction $\psi(\mathbf{r})$ is then simply a coefficient saying how much of the basis vector $|\mathbf{r}\rangle$ (the spatial representation of which is a Dirac delta centred on the position \mathbf{r}) to include in the overall state vector. What we have *not* done is chosen a subset of these Dirac delta basis functions¹⁶ as our basis. This would be very strange—our representation of the wavefunction would allow it to have a value at one gridpoint, and at the next gridpoint, but not in between. Spatially separated Dirac deltas do not spatially overlap at all; the

¹⁴For the sake of example— 256×256 is a more realistic minimum.

¹⁵One for each position within the two dimensional space we're representing.

¹⁶Strictly, distributions, not functions, but “basis distributions” just doesn't have the right ring to it.

matrix elements of the kinetic energy operator:

$$\langle \mathbf{r}_i | \hat{K} | \mathbf{r}_j \rangle = \int \delta(\mathbf{r} - \mathbf{r}_i) \left(-\frac{\hbar^2}{2m} \nabla^2 \right) \delta(\mathbf{r} - \mathbf{r}_j) d\mathbf{r} \quad (3.57)$$

would all be zero for $i \neq j$, disallowing any flow of amplitude from one point in space to another by virtue of it not being able to pass through the intervening points. Neither have we chosen a set of two-dimensional boxcar functions centred on each gridpoint with width Δx in each direction. These cover all space in between gridpoints, but are no good because they are not twice differentiable everywhere, and hence the kinetic energy operator's matrix elements cannot be evaluated. No, neither of these bases will do. To interpret our spatial grid as a basis, we need a set of functions $[FUNC_{ij}(\mathbf{r})]$ (where i and j are the indices of the gridpoints in the x and y directions respectively) that have unit norm, are nonzero only at one gridpoint and are zero at all others, and are twice differentiable everywhere in our spatial region. Infinite choices present themselves to us, differing only in their incompleteness—the choice of which state vectors they will and won't be able to represent. A sensible choice is that we want to be able to represent the state vectors whose wavefunctions do not change much between adjacent gridpoints, and we are happy for the necessary incompleteness of our basis to exclude wavefunctions with any sort of structure in between gridpoints.

The discrete Fourier transform to the rescue

It turns out that discretising space in this way can indeed be equivalent to choosing an entirely sensible basis. This is made clearer by thinking in terms of what we have done in Fourier space, which I'll quickly go through now.

One possible basis for representing all possible state vectors is the Fourier basis $\{|\mathbf{k}_{ij}\rangle\}$. With it, any state vector (whose wavefunction is nonzero only within the 2D region) can be represented as the sum of basis vectors whose wavefunctions are 2D plane waves, also localised to the 2D region:

$$\langle \mathbf{r} | \mathbf{k}_{ij} \rangle = \begin{cases} \frac{1}{\sqrt{A}} e^{i\mathbf{k}_{ij} \cdot \mathbf{r}} & (\mathbf{r} \text{ within 2D region}) \\ 0 & (\mathbf{r} \text{ not within 2D region}), \end{cases} \quad (3.58)$$

where A is the area of the 2D region and the wavevector of each plane wave is

$$\mathbf{k}_{ij} = \left[\frac{2\pi i}{L_x}, \frac{2\pi j}{L_y} \right]^T, \quad (3.59)$$

where i and j are (possibly negative) integers. Any state vector localised to the 2D region can then be written as the infinite sum:

$$|\psi\rangle = \sum_{i=0}^{\infty} \sum_{j=0}^{\infty} \langle \mathbf{k}_{ij} | \psi \rangle |\mathbf{k}_{ij}\rangle \quad (3.60)$$

$$\Rightarrow \psi(\mathbf{r}) = \begin{cases} \sum_{i=0}^{\infty} \sum_{j=0}^{\infty} \langle \mathbf{k}_{ij} | \psi \rangle \frac{1}{\sqrt{A}} e^{i\mathbf{k}_{ij} \cdot \mathbf{r}} & (\mathbf{r} \text{ within 2D region}) \\ 0 & (\mathbf{r} \text{ not within 2D region}). \end{cases} \quad (3.61)$$

So $\{\langle \mathbf{k}_{ij} | \psi \rangle\}$ are simply the coefficients of the 2D Fourier series of $\psi(\mathbf{r})$.

What does this have to do with our discretised space? These basis functions $\{\langle \mathbf{r} | \mathbf{k}_{ij} \rangle\}$ don't have the required properties for a discrete basis. For one, there are an infinite number of them, and we require 25. Secondly, all of them are nonzero everywhere within the 2D region, whereas we require each basis function to be nonzero at exactly one of our 25 gridpoints.

rev: 45 (b37fd8d3e6c7)
author: Chris Billington
date: Fri Mar 17 17:54:14 2017 -0400
summary: Almost completed commutation error figure.

We can solve the first problem by truncating the Fourier series. By only including basis vectors $|\mathbf{k}_{ij}\rangle$ for which:

$$\begin{cases} i \in [-\frac{N_x}{2}, \frac{N_x}{2} - 1] & (N_x \text{ even}) \\ i \in [-\frac{N_x-1}{2}, \frac{N_x-1}{2}] & (N_x \text{ odd}) \end{cases} \quad (3.62)$$

and

$$\begin{cases} j \in [-\frac{N_y}{2}, \frac{N_y}{2} - 1] & (N_y \text{ even}) \\ j \in [-\frac{N_y-1}{2}, \frac{N_y-1}{2}] & (N_y \text{ odd}) \end{cases} \quad (3.63)$$

we include only the N_x and N_y (both equal to 5 in our example) longest wavelengths in each respective spatial dimension. This is a sensible truncation with a physically meaningful interpretation. By making it, we are no longer able to represent state vectors with short wavelength components. Because the kinetic energy operator, when represented in the Fourier basis, is:

$$\langle \mathbf{k}_{ij} | \hat{K} | \mathbf{k}_{i'j'} \rangle = \frac{\hbar^2 k^2}{2m} \delta_{ii'} \delta_{jj'}, \quad (3.64)$$

where $k = |\mathbf{k}_i|$, by excluding basis vectors with larger wavevectors, we are excluding state vectors with large kinetic energy. Thus the truncation is a kinetic energy cutoff, and is an accurate approximation whenever a simulation is such that the system is unlikely to obtain kinetic energies above the cutoff.¹⁷

Now we have 25 basis vectors—a discrete Fourier basis—but their spatial wavefunctions still don't have the property of being nonzero only at a single gridpoint each. On the contrary, each plane wave has a constant amplitude everywhere in space. But consider the following superposition of Fourier basis vectors:

$$|\mathbf{r}_{ij}\rangle = \sum_{i'j'} e^{-i\mathbf{k}_{i'j'} \cdot \mathbf{r}_{ij}} |\mathbf{k}_{i'j'}\rangle \quad (3.65)$$

with $\mathbf{r}_{ij} = (i\Delta x, j\Delta y)^T$ and $i, j \in [0, 4]$. This is simply a unitary transformation of the truncated Fourier basis, with the unitary transformation matrix elements:

$$\hat{U}_{\text{DFT2}; i'j'; ij} = \langle \mathbf{k}_{i'j'} | \mathbf{r}_{ij} \rangle = e^{-i\mathbf{k}_{i'j'} \cdot \mathbf{r}_{ij}}. \quad (3.66)$$

This transformation is in fact a discrete Fourier transform (hence the subscript), and the basis vectors $\{|\mathbf{r}_{ij}\rangle\}$ have spatially localised wavefunctions that are nonzero only at one of the spatial gridpoints, so we refer to them as a discrete real-space basis. State vectors and operators can be transformed from their discrete Fourier space representation to their discrete real-space representation and back using the unitary \hat{U}_{DFT2} :

$$\langle \mathbf{r}_{ij} | \psi \rangle = \sum_{i'j'} \hat{U}_{\text{DFT2}; ij; i'j'}^\dagger \langle \mathbf{k}_{i'j'} | \psi \rangle \quad (3.67)$$

$$\langle \mathbf{k}_{ij} | \psi \rangle = \sum_{i'j'} \hat{U}_{\text{DFT2}; i'j'; ij} \langle \mathbf{r}_{i'j'} | \psi \rangle \quad (3.68)$$

[TODO OPERATOR TRANSFORMATIONS ONCE INDEXING IMPROVED AND VECTOR REPRESENTATIONS INTRODUCED]

The spatial representation of the basis vectors $\{|\mathbf{r}_{ij}\rangle\}$ can be computed using (3.58) as:

$$\phi_{ij}(\mathbf{r}) = \langle \mathbf{r} | \mathbf{r}_{ij} \rangle = \sum_{i'j'} e^{-i\mathbf{k}_{i'j'} \cdot \mathbf{r}_{ij}} \langle \mathbf{r} | \mathbf{k}_{i'j'} \rangle \quad (3.69)$$

$$\Rightarrow \phi_{ij}(\mathbf{r}) = \begin{cases} \sum_{i'j'} \frac{1}{\sqrt{A}} e^{i\mathbf{k}_{i'j'} \cdot (\mathbf{r} - \mathbf{r}_{ij})} & (\mathbf{r} \text{ within 2D region}) \\ 0 & (\mathbf{r} \text{ not within 2D region}), \end{cases} \quad (3.70)$$

¹⁷Because a *square* region in Fourier space is being carved out, by limiting each of k_x and k_y to finite ranges rather than the total wavenumber $k = \sqrt{k_x^2 + k_y^2}$, there is no single kinetic energy cutoff so to speak. Nonetheless there is a maximum wavenumber $k_{\text{max}} = \min(\{|k_x|\} \cup \{|k_y|\})$ defining a kinetic energy cutoff $K_{\text{max}} = \hbar^2 k_{\text{max}}^2 / (2m)$ below which kinetic energies definitely are representable and above which they may not be.

and are plotted in [TODO MAKE FIGURE].

These functions are sometimes called *periodic sinc functions*, or *band-limited delta functions* [CITE]. Each of them is zero at all of our gridpoints except one, and they form an orthonormal basis set. They satisfy all of our requirements to be a basis corresponding to our gridded discretisation of space. Thus, the approach of discretising space on a grid is indeed equivalent to choosing a (necessarily incomplete) orthonormal basis in which to work.

One thing to note is that these functions are periodic. By using the Fourier basis in the way we have to restrict our basis to cover only a finite region of both Fourier space and real space, we have necessarily imposed periodicity on the problem. This periodicity shows itself when we compute matrix elements of operators in this basis - if we compute the kinetic energy operator's matrix elements for example, it will couple basis states across the boundary of the region, resulting in spatial periodicity—a wavepacket moving rightward through the right boundary will emerge moving rightward from the left boundary.

Perhaps less obviously, the basis is also periodic in Fourier space, and so a wavepacket moving out of the region of Fourier space simulated will also wrap around to the opposite side of Fourier space. In real space, this may appear as a wavepacket undergoing acceleration only to suddenly reverse its velocity as if reflecting off a barrier [SEE FIG TODO FOR EXAMPLE]. This effect is entirely unphysical¹⁸ and should be taken as a sign that the spatial grid is not fine enough for the dynamics being simulated.

¹⁸With the possible exception of the region of Fourier space being simulated corresponding to the first Brillouin zone of a lattice potential, in which case these velocity reversals are Bloch oscillations.

¹⁹Or rather, a state vector's projection onto the subspace being simulated.

Matrix elements using DFT basis

We now have a finite basis $\{|r_{ij}\rangle\}$ that matches our intuitions somewhat for representing a wavefunction at a set of gridpoints. A state vector¹⁹ can be represented as a linear sum of these basis vectors, with the coefficient for each one simply being equal to the value of that state vector's wavefunction at the gridpoint where that basis vector is nonzero:

$$|\psi\rangle = \sum_{i,j} c_{i,j} |r_{i,j}\rangle, \quad (3.71)$$

where

$$c_{i,j} = \langle r_{i,j} | \psi \rangle = \psi(r_{i,j}). \quad (3.72)$$

Armed with a basis, we can now proceed to calculate matrix elements of the Hamiltonian, and then proceed to solve the differential equation [TODO EQREF 3.3] to determine how the coefficients $\{c_{i,j}\}$ evolve in time.

The specific properties of our basis make it quite useful for a range of common Hamiltonians. For example, let's take the single particle Schrödinger Hamiltonian:

$$\hat{H}_{\text{Schrö}} = -\frac{\hbar^2 \hat{k}^2}{2m} + V(\hat{r}), \quad (3.73)$$

where $\hat{k} = |\hat{\mathbf{k}}|$.

The two terms, kinetic and potential, are each diagonal in different bases. The kinetic term is diagonal in the Fourier basis:

$$\langle \mathbf{k}' | -\frac{\hbar^2 \hat{k}^2}{2m} | \mathbf{k} \rangle = -\frac{\hbar^2 k^2}{2m} \delta(\mathbf{k} - \mathbf{k}'), \quad (3.74)$$

where $k = |\mathbf{k}|$, and the potential term is diagonal in the spatial basis:

$$\langle \mathbf{r}' | V(\hat{r}) | \mathbf{r} \rangle = V(\mathbf{r}) \delta(\mathbf{r} - \mathbf{r}'). \quad (3.75)$$

Equivalent relations hold for our discrete Fourier and spatial basis:

$$\langle \mathbf{k}_{i'j'} | -\frac{\hbar^2 \hat{k}^2}{2m} | \mathbf{k}_{ij} \rangle = -\frac{\hbar^2 k_{ij}^2}{2m} \delta_{i'i} \delta_{j'j}, \quad (3.76)$$

$$\langle \mathbf{r}_{i'j'} | V(\hat{\mathbf{r}}) | \mathbf{r}_{ij} \rangle = V(\mathbf{r}_{ij}) \delta_{i'i} \delta_{j'j}. \quad (3.77)$$

But to obtain our differential equation, we need all the matrix elements of $\hat{H}_{\text{Schrö}}$ in a single basis.

3.4.2 Finite differences

- Simple, equal to fixed order approximation to fourier method.
- But can be made non-periodic
- Computationally efficient compared to FFTs in Runge–Kutta.
- Computationally efficient compared to FFTs in split-step (banded matrices amenable to splitting into sum of two block-diagonal matrices).
- Parallelisable in both cases, with number of points needing to be exchanged related to the order of the finite difference (2nd order, 1 point, 4th order, 2 points etc).
- Single-core efficiency compared to FFTs not observable in practice on current computers—to see it you need more points than fit in CPU cache and so both of them are limited by memory bandwidth and $\mathcal{O}(n)$ with big coefficient. But FD are parallelisable without shared data, whereas parallel FFTs scale poorly - the amount of data needing to be sent per node increases with the number of nodes. But, on a GPU where all data is available, parallel FFTs can be pretty good.
- Also good compared to FFTs in that many problems are not actually periodic, and imposing periodicity on them can cause problems - finite differences give you a fair bit of freedom to make your own boundary conditions.

3.4.3 The finite element discrete variable representation

- Summarise, don't go into detail. Just a different method of spatial discretisation.
- Splits space into 'elements'. Briefly mention what these are good for - funky boundary conditions and irregular grids mostly
- Represents state vector within each element using interpolating polynomials - they're a basis but they're not an orthonormal one. Each one is zero all points in each element except one. To get coefficients in this basis you get the wavefunction's values at the specific points in space (you can't just do a projection, because the basis isn't orthonormal - you'd get a state vector with >1 norm if you did that). To reconstruct a wavefunction again you sum the interpolating polynomials with their coefficients.
- Benefit of finite elements in general, other than boundary conditions and variable grids is that you can choose basis functions within elements that conserve some known conserved quantities, and hence you can make geometric integrators.
- Differential operators can be computed using the quadrature rule, and then you can solve using Runge-Kutta or split-step. The main paper on all this [CITE] uses fourth order split-step.

rev: 45 (b37fd8d3e6c7)
author: Chris Billington
date: Fri Mar 17 17:54:14 2017 -0400
summary: Almost completed commutation error figure.

- For the Schrodinger and Schrodinger-like equations, purported benefit other than irregular gridding and boundary conditions is that you only need to exchange one point between elements, speeding up parallel implementations.
- Go into why that actually doesn't help:
- Conceptually I like to think of DVR as non-central finite differences on an irregular grid. Finite differences are also based on interpolating polynomials. Central finite differences of say, 6th order accuracy would require sending four points across compute-node boundaries every time you want to apply an operator to a state vector. But, non-central finite differences within individual elements, instead of central finite differences everywhere, can make it such that within elements, points need every other point in order to compute a differential operator - but they only require one point across element boundaries. The differential operators are still same order accuracy in δx . But, now they're subject to Gibbs'/Runge's phenomenon. So, you solve this by making the points unequally spaced. [Such and such theorem] says that you optimally suppress the oscillations near the element boundaries if the point spacing scales like [however it scales]. So you space the points unevenly like that, recompute your differential operators based on what the interpolating polynomials now look like, and you have a DVR basis. If you force points to be on element boundaries and do some tricks to join elements together, you now have an FEDVR basis.
- The paper compares 6th order [and other order] FEDVR to 2nd order finite differences for accuracy in representing the 2D SHO groundstate. FEDVR wins the comparison. But, i think it's not a fair comparison because they only used second order central finite differences. 6th order central finite differences are just as accurate as 6th order FEDVR.
- But if you use 6th order central finite differences, you have to pass 4x more points at compute-node boundaries compared to FEDVR. So that means FEDVR parallelises better, right? Wrong. Not for time-evolution, and not for the Schrodinger equation. Maximum timestep you can take (regardless of RK or split-step) is set by the kinetic term and is intuitive - you can't take timesteps longer than the time it takes the fastest mode to move the smallest grid spacing.
- FEDVR has *smaller minimum grid spacing*. It requires smaller timesteps. How much smaller? [SHOW CALCULATION] Enough to mean that you have to take 16x as many timesteps compared to FD. So you thought you were sending four times less data compared to central finite differences, but you're actually sending four times more, because you are only sending four times less per timestep - and you are taking sixteen times as many timesteps.
- So unless you're using it in order to have irregular grids or strange boundary conditions, FEDVR provides little benefit for time-evolving Schrodinger-like equations. Finite differences can be used on irregular grids too [CITE]

3.4.4 Harmonic oscillator basis functions

[Another way of discretising space. Not a grid at all. Useful in, well, harmonic and approximately harmonic potentials, or (well, equivalently) when Hamiltonian is sparse in the SHO eigenbasis. Otherwise not great - without FFTs, applying the Hamiltonian means big, dense matrices - slow.]

rev: 45 (b37fd8d3e6c7)
author: Chris Billington
date: Fri Mar 17 17:54:14 2017 -0400
summary: Almost completed commutation error figure.

3.5 Finding ground states

3.5.1 Imaginary time evolution

[Summarise ITEM]

3.5.2 Successive over-relaxation

[Summarise SOR]

3.5.3 Generalisation to excited states via Gram–Schmidt orthonormalisation

Directly diagonalising a Hamiltonian can be costly in a spatial basis. Another approach is to find the ground state using one of the above techniques, and then repeat the process, subtracting off the wavefunction's projection onto the already found ground state at every step. This yields the lowest energy state that is orthogonal to the first - i.e. the first excited state. Repeating the process, but subtracting off *both* eigenstates found so far, then yields the second excited state and so forth. This is simply the Gram-Schmidt process for finding orthonormal vectors, with the additional step of relaxing each vector to the lowest possible energy for each one - this ensures the eigenstates of the Hamiltonian are produced, rather than a different orthogonal basis. Extra conditions can be imposed on the wavefunction at each relaxation step in order to obtain particular solutions in the case of degenerate eigenstates. For example, a phase winding can be imposed in order to obtain a particular harmonic oscillator state - otherwise this process produces an arbitrary superposition of basis states that have equal energy.

3.6 Fourth order Runge–Kutta in an instantaneous local interaction picture

Consider the differential equation for the components of a state vector $|\psi(t)\rangle$ in a particular basis with basis vectors $|n\rangle$. This might simply be the Schrödinger equation, or perhaps some sort of nonlinear or other approximate, effective or phenomenological equation not corresponding to pure Hamiltonian evolution. Though they may have additional terms, such equations are generally of the form:

$$\frac{d}{dt} \langle n|\psi(t)\rangle = -\frac{i}{\hbar} \sum_m \langle n|\hat{H}(t)|m\rangle \langle m|\psi(t)\rangle, \quad (3.78)$$

where $\langle n|\hat{H}(t)|m\rangle$ are the matrix elements in that basis of the Hamiltonian $\hat{H}(t)$, which in general can be time dependent, or even a function of $|\psi(t)\rangle$, depending on the exact type of equation in use. If $\hat{H}(t)$ is almost diagonal in the $|n\rangle$ basis, then the solution to (3.78) is dominated by simple dynamical phase evolution, that is:

$$|\psi(t)\rangle \approx \sum_m e^{-\frac{i}{\hbar} E_m t} |m\rangle, \quad (3.79)$$

where E_m is the energy eigenvalue corresponding to the eigenstate $|m\rangle$.

A transformation into an interaction picture (IP) [23, p318] is commonly used to treat this part of the evolution analytically, before solving the remaining dynamics with further analytics or numerics. For numerical methods, integration in the interaction picture allows one to use larger integration timesteps, as one does not need to resolve the fast oscillations around the complex plane due to this dynamical phase.

rev: 45 (b37fd8d3e6c7)
 author: Chris Billington
 date: Fri Mar 17 17:54:14 2017 -0400
 summary: Almost completed commutation error figure.

²⁰For example, a spatial basis which allows for partitioning the integration region over multiple nodes on a cluster or cores on a GPU.

Choosing an interaction picture typically involves diagonalising the time-independent part of a Hamiltonian, and then proceeding in the basis in which that time-independent part is diagonal. However, often one has a good reason to perform computations in a different basis, in which the time independent part of the Hamiltonian is only approximately diagonal,²⁰ and transforming between bases may be computationally expensive (involving large matrix-vector multiplications). Furthermore, the Hamiltonian may change sufficiently during the time interval being simulated that the original time-independent Hamiltonian no longer dominates the dynamics at later times. In both these cases it would still be useful to factor out the time-local oscillatory dynamics in whichever basis is being used, in order to avoid taking unreasonably small timesteps.

To that end, suppose we decompose $\hat{H}(t)$ into diagonal and non-diagonal (in the $|n\rangle$ basis) parts at each moment in time:

$$\hat{H}(t) = \hat{H}_{\text{diag}}(t) + \hat{H}_{\text{nondiag}}(t), \quad (3.80)$$

and use the diagonal part at a specific time $t = t'$ to define a time-independent Hamiltonian:

$$\hat{H}'_0 = \hat{H}_{\text{diag}}(t'), \quad (3.81)$$

which is diagonal in the $|n\rangle$ basis. We can then use then use \hat{H}'_0 to define an interaction picture state vector:

$$|\psi'_I(t)\rangle = e^{\frac{i}{\hbar}(t-t')\hat{H}'_0} |\psi(t)\rangle, \quad (3.82)$$

which obeys the differential equation:

$$\frac{d}{dt} |\psi'_I(t)\rangle = e^{\frac{i}{\hbar}(t-t')\hat{H}'_0} \frac{d}{dt} |\psi(t)\rangle + \frac{i}{\hbar} \hat{H}'_0 |\psi'_I(t)\rangle, \quad (3.83)$$

where:

$$|\psi(t)\rangle = e^{-\frac{i}{\hbar}(t-t')\hat{H}'_0} |\psi'_I(t)\rangle \quad (3.84)$$

is the original Schrödinger picture (SP) state vector.

This transformation is exact, no approximations or assumptions have been made. If indeed the dynamics of $|\psi(t)\rangle$ in the given basis are dominated by fast oscillating dynamical phases, that is, the diagonals of $\hat{H}_{\text{diag}}(t)$ are much greater than all matrix elements of $\hat{H}_{\text{nondiag}}(t)$ in the $|n\rangle$ basis, then solving the differential equation (3.83) for $|\psi'_I(t)\rangle$ should allow one to use larger integration timesteps than solving (3.78) directly. And if not, then it should do no harm other than the (small) computational costs of computing some extra scalar exponentials.

Equation (3.82) defines an *instantaneous* interaction picture, in that it depends on the dynamics at a specific time $t = t'$, and can be recomputed repeatedly throughout a computation in order to factor out the fast dynamical phase evolution even as the oscillation rates change over time. It is *local* in that H'_0 is diagonal in the $|n\rangle$ basis, which means that transformations between Schrödinger picture and interaction picture state vectors involves ordinary, elementwise exponentiation of vectors, rather than matrix products. Thus (3.82), (3.83) and (3.84) can be written componentwise as:

$$\langle n | \psi'_I(t) \rangle = e^{i(t-t')\omega'_n} \langle n | \psi(t) \rangle, \quad (3.85)$$

$$\frac{d}{dt} \langle n | \psi'_I(t) \rangle = e^{i(t-t')\omega'_n} \frac{d}{dt} \langle n | \psi(t) \rangle + i\omega'_n \langle n | \psi'_I(t) \rangle, \quad (3.86)$$

and:

$$\langle n|\psi(t)\rangle = e^{-i(t-t')\omega_n'} \langle n|\psi_1'(t')\rangle, \quad (3.87)$$

where we have defined:

$$\omega_n' = \frac{1}{\hbar} \langle n|\hat{H}_0'|n\rangle \quad (3.88)$$

This is in contrast to fourth order Runge–Kutta in the interaction picture (RK4IP) [24], in which the interaction picture uses the Fourier basis and thus transforming to and from it involves fast Fourier transforms (FFTs). RK4IP was developed to augment computations in which FFTs were already in use for evaluating spatial derivatives, and so its use of FFTs imposes no additional cost. Nonetheless, an interaction picture based on the kinetic term of the Schrödinger equation (which is the term of the Hamiltonian that RK4IP takes as its time-independent part) may not be useful if that term does not dominate the Hamiltonian, as in the case of a Bose–Einstein condensate in the Thomas–Fermi limit. We compare the two methods below.

3.6.1 Algorithm

The *fourth order Runge–Kutta in an instantaneous local interaction picture* RK4ILIP algorithm is now obtained by using (3.82) to define a new interaction picture at the beginning of each fourth-order Runge–Kutta (RK4) integration timestep. The differential equation and initial conditions supplied to the algorithm are in the ordinary Schrödinger picture, and the interaction picture is used only within a timestep, with the Schrödinger picture state vector returned at the end of each timestep. Thus differential equations need not be modified compared to if ordinary RK4 were being used, and the only modification to calling code required is for a function to compute and return ω_n' .

Being based on fourth order Runge–Kutta integration, this new method enjoys all the benefits of a workhorse method that is time-proven, and—as evidenced by its extremely widespread use—at a sweet-spot of ease of implementation, accuracy, and required computing power [25].

Below is the resulting algorithm for performing one integration timestep. It takes as input the time t_0 at the start of the timestep, the timestep size Δt , an array ψ_0 containing the components $\{\langle n|\psi(t_0)\rangle\}$ of the state vector at time t_0 , a function $F(t, \psi)$ which takes a time and (the components of) a state vector and returns an array containing the time derivative of each component, and a function $G(t, \psi)$ which takes the same inputs and returns an array containing the interaction picture oscillation frequency ω_n for each component at that time.

For example, for the case of the Gross–Pitaevskii equation [26] in the spatial basis $\psi(\mathbf{r}, t) = \langle \mathbf{r}|\psi(t)\rangle$, these would be:

$$F(t, \psi(\mathbf{r}, t)) = -\frac{i}{\hbar} \left[\underbrace{-\frac{\hbar^2}{2m} \nabla^2}_{\hat{H}_{\text{nondiag}}} + \underbrace{V(\mathbf{r}, t) + g|\psi(\mathbf{r}, t)|^2}_{\hat{H}_{\text{diag}}} \right] \psi(\mathbf{r}, t), \quad (3.89)$$

and

$$G(t, \psi(\mathbf{r}, t)) = \frac{1}{\hbar} \left[\underbrace{V(\mathbf{r}, t) + g|\psi(\mathbf{r}, t)|^2}_{\hat{H}_{\text{diag}}} \right]. \quad (3.90)$$

Note that each symbol in bold in the algorithm below denotes an array containing one element for each basis vector $|n\rangle$, subscripts denote the different stages of RK4, and

rev: 45 (b37fd8d3e6c7)
author: Chris Billington
date: Fri Mar 17 17:54:14 2017 -0400
summary: Almost completed commutation error figure.

all arithmetic operations between arrays are elementwise²¹. The only opportunity for non-elementwise operations to occur is within F , which contains the details (via \hat{H}_{nondiag}) of any couplings between basis states for whatever system of equations is being solved, for example, using FFTs or finite differences to evaluate the Laplacian in (3.89).

Algorithm 1 RK4ILIP

```

1: function RK4ILIP( $t_0, \Delta t, \psi_0, F$ )
2:    $f_1 \leftarrow F(t_0, \psi_0)$  ▷ First evaluation of Schrödinger picture DE
3:    $\omega \leftarrow G(t_0, \psi_0)$  ▷ Oscillation frequencies:  $\hbar\omega_n = \langle n | \hat{H}_{\text{diag}}(t_0) | n \rangle$ 
4:    $k_1 \leftarrow f_1 + i\omega\psi_0$  ▷ Evaluate (3.86) with  $t - t' = 0$ 
5:    $\phi_1 \leftarrow \psi_0 + k_1 \frac{\Delta t}{2}$  ▷ First RK4 estimate of IP state vector, at  $t = t_0 + \frac{\Delta t}{2}$ 
6:    $\psi_1 \leftarrow e^{-i\omega \frac{\Delta t}{2}} \phi_1$  ▷ Convert first estimate back to SP with (3.87)
7:    $f_2 \leftarrow F(t_0 + \frac{\Delta t}{2}, \psi_1)$  ▷ Second evaluation of Schrödinger picture DE
8:    $k_2 \leftarrow e^{i\omega \frac{\Delta t}{2}} f_2 + i\omega\phi_1$  ▷ Evaluate (3.86) with  $t - t' = \frac{\Delta t}{2}$ 
9:    $\phi_2 \leftarrow \psi_0 + k_2 \frac{\Delta t}{2}$  ▷ Second RK4 estimate of IP state vector, at  $t = t_0 + \frac{\Delta t}{2}$ 
10:   $\psi_2 \leftarrow e^{-i\omega \frac{\Delta t}{2}} \phi_2$  ▷ Convert second estimate back to SP with (3.87)
11:   $f_3 \leftarrow F(t_0 + \frac{\Delta t}{2}, \psi_2)$  ▷ Third evaluation of Schrödinger picture DE
12:   $k_3 \leftarrow e^{i\omega \frac{\Delta t}{2}} f_3 + i\omega\phi_2$  ▷ Evaluate (3.86) with  $t - t' = \frac{\Delta t}{2}$ 
13:   $\phi_3 \leftarrow \psi_0 + k_3 \Delta t$  ▷ Third RK4 estimate of IP state vector, at  $t = t_0 + \Delta t$ 
14:   $\psi_3 \leftarrow e^{-i\omega \Delta t} \phi_3$  ▷ Convert third estimate back to SP with (3.87)
15:   $f_4 \leftarrow F(t_0 + \Delta t, \psi_3)$  ▷ Fourth evaluation of Schrödinger picture DE
16:   $k_4 \leftarrow e^{i\omega \Delta t} f_4 + i\omega\phi_3$  ▷ Evaluate (3.86) with  $t - t' = \Delta t$ 
17:   $\phi_4 \leftarrow \psi_0 + \frac{\Delta t}{6} (k_1 + 2k_2 + 2k_3 + k_4)$  ▷ Fourth RK4 estimate, at  $t = t_0 + \Delta t$ 
18:   $\psi_4 \leftarrow e^{-i\omega \Delta t} \phi_4$  ▷ Convert fourth estimate back to SP with (3.87)
19:  return  $\psi_4$  ▷ Return the computed SP state vector at  $t = t_0 + \Delta t$ 
20: end function

```

Note on imaginary time evolution

When RK4ILIP is used for imaginary time evolution (ITE) [27], the oscillation frequencies ω may have a large imaginary part. If the initial guess is different enough from the ground state, then the exponentials in (3.85), (3.86) and (3.87) may result in numerical overflow. To prevent this, one can define a clipped copy of ω ,

$$\omega_{\text{clipped}} = \text{Re}(\omega) + i \begin{cases} -\frac{\log X}{\Delta t} & \text{Im}(\omega)\Delta t < -\log X \\ \text{Im}(\omega) & -\log X \leq \text{Im}(\omega)\Delta t \leq \log X \\ \frac{\log X}{\Delta t} & \text{Im}(\omega)\Delta t > \log X \end{cases}, \quad (3.91)$$

where X is very large but less than the largest representable floating-point number, and use ω_{clipped} in the exponents instead. In the below results I used RK4ILIP with ITE to smooth initial states of a Bose–Einstein condensate after a phase printing, and performed clipping with ²² $\log X = 400$.

This clipped version of ω should be used in all exponents in the above algorithm, but only in exponents—not in the second term of (3.86). If it is used everywhere then all we have done is chosen a different (less useful) interaction picture, and the algorithm will still overflow. By clipping only the exponents, we produce temporarily “incorrect” evolution²³, limiting the change in magnitude of each component of the state vector to a factor of X per step (remembering that X is very large). This continues for the few steps that it takes ITE to get all components of the state vector to within a factor of X of the

²² 400 being about half the largest (base e) exponent representable in double-precision floating point.

²³ Of no concern since we are using ITE as a relaxation method, and are not interested in intermediate states. Only the final state’s correctness concerns us.

ground state, after which no clipping is necessary and convergence to the ground state proceeds as normal, subject to the ordinary limitations on which timesteps may be used with ITE.

3.6.2 Domain of improvement over other methods

For simulations in the spatial basis, RK4ILIP treats the spatially local part of the Hamiltonian analytically to first order, and hence can handle larger potentials than ordinary RK4. However, since a global energy offset can be applied to any potential with no physically meaningful change in the results, ordinary RK4 can also handle large potentials — if they are large due to a large constant term which can simply be subtracted off.

So RK4ILIP is only of benefit in the case of large *spatial variations* in the potential. Only one constant can be subtracted off potentials without changing the physics — subtracting a spatially varying potential would require modification of the differential equation in the manner of a gauge transformation in order to leave the system physically unchanged²⁴.

However that's not quite all: large spatial variation in potentials often comes with the prospect of the potential energy turning into kinetic energy, in which case RK4ILIP is also of little benefit, since in order to resolve the dynamical phase due to the large kinetic term, it would require timesteps just as small as those which ordinary RK4 would need to resolve the dynamical phase evolution from the large potential term.

This leaves RK4ILIP with an advantage only in the case of large spatial variations in the potential that do not lead to equally large kinetic energies. Hence the examples I show in the next section are ones in which the condensate is trapped in a steep potential well—the trap walls are high and hence involve large potentials compared to the interior, but do not lead to large kinetic energies because the condensate is trapped close to its ground state.

The Fourier split-step (FSS) method [28] (see section [TODO]) also models dynamical phases due to the potential analytically to low order. As such it is also quite capable of modeling large potentials. However, it requires that all operators be diagonal in either the spatial basis or the Fourier basis [28]. Therefore BECs in rotating frames, due to the Hamiltonian containing an angular momentum operator, are not amenable to simulation with FSS²⁵.

This use of FFTs in both the FSS and RK4IP methods necessarily imposes periodic boundary conditions on a simulation, which may not be desirable. By contrast, if different boundary conditions are desired, finite differences instead of FFTs can be used to evaluate spatial derivatives in the RK4 and RK4ILIP methods, so long as a sufficiently high-order finite difference scheme is used so as not to unacceptably impact accuracy.

Along with the ability to impose arbitrary boundary conditions, finite differences require only local data, that is, only points spatially close to the point being considered need be known in order to evaluate derivatives there. This makes finite differences amenable to simulation on cluster computers [29, p100], with only a small number of points (depending on the order of the scheme) needing to be exchanged at node-boundaries each step. By contrast, FFT based derivatives require data from the entire spatial region. Whilst this can still be parallelised on a GPU, where all the data is available, it cannot be done on a cluster without large amounts of data transfer between nodes [30]. Thus, RK4 and RK4ILIP, being implementable with finite difference schemes, are considerably friendlier to cluster computing.

Table 3.1 summarises the capabilities of the four methods considered in the following results section. RK4ILIP is the only method capable of modelling a large spatial variation in the potential term whilst being locally parallelisable, and supporting arbitrary operators and boundary conditions.

²⁴Though a numerical solution based on analytically gauging away potentials at each timestep might be equally as fruitful as RK4ILIP.

²⁵Split-step with more than these two bases is however possible in other schemes such as the finite element discrete variable representation [21]—each operator can be diagonalised and exponentiated locally in each element and applied as a (relatively small) matrix multiplication rather than using FFTs.

| Method | RK4 | RK4IP | RK4ILIP | FSS |
|-------------------------------|---------------------------|---------------------------|---------------------------|---------------------------|
| Error | $\mathcal{O}(\Delta t^4)$ | $\mathcal{O}(\Delta t^4)$ | $\mathcal{O}(\Delta t^4)$ | $\mathcal{O}(\Delta t^2)$ |
| FFTs per step | 4 | 4 | 4 | 2 |
| Large ΔV | No | No | Yes | Yes |
| Large kinetic term | No | Yes | No | Yes |
| Arbitrary operators | Yes | Yes [†] | Yes | No |
| Locally parallelisable | Yes | No | Yes | No |
| Arbitrary boundary conditions | Yes | No | Yes | No |

Table 3.1: Advantages and disadvantages of four timestepping methods for simulating Bose–Einstein condensates. *Large ΔV* refers to whether the method can simulate potentials that vary throughout space by an amount larger than the energy scale $2\pi\hbar/\Delta t$ associated with the simulation timestep Δt . *Arbitrary operators* refers to whether the method permits operators that are not diagonal in either the spatial or Fourier basis, such as angular momentum operators. *Locally parallelisable* means the method can be formulated so as to use only spatially nearby points in evaluating operators, and thus is amenable to parallelisation by splitting the simulation over multiple cores in the spatial basis. [†] Whilst one can include arbitrary operators within the RK4IP method, only operators diagonal in Fourier space can be analytically treated the way RK4IP treats the kinetic term, and so there is no advantage for these terms over ordinary RK4.

rev: 45 (b37fd8d3e6c7)
author: Chris Billington
date: Fri Mar 17 17:54:14 2017 -0400
summary: Almost completed commutation error figure.

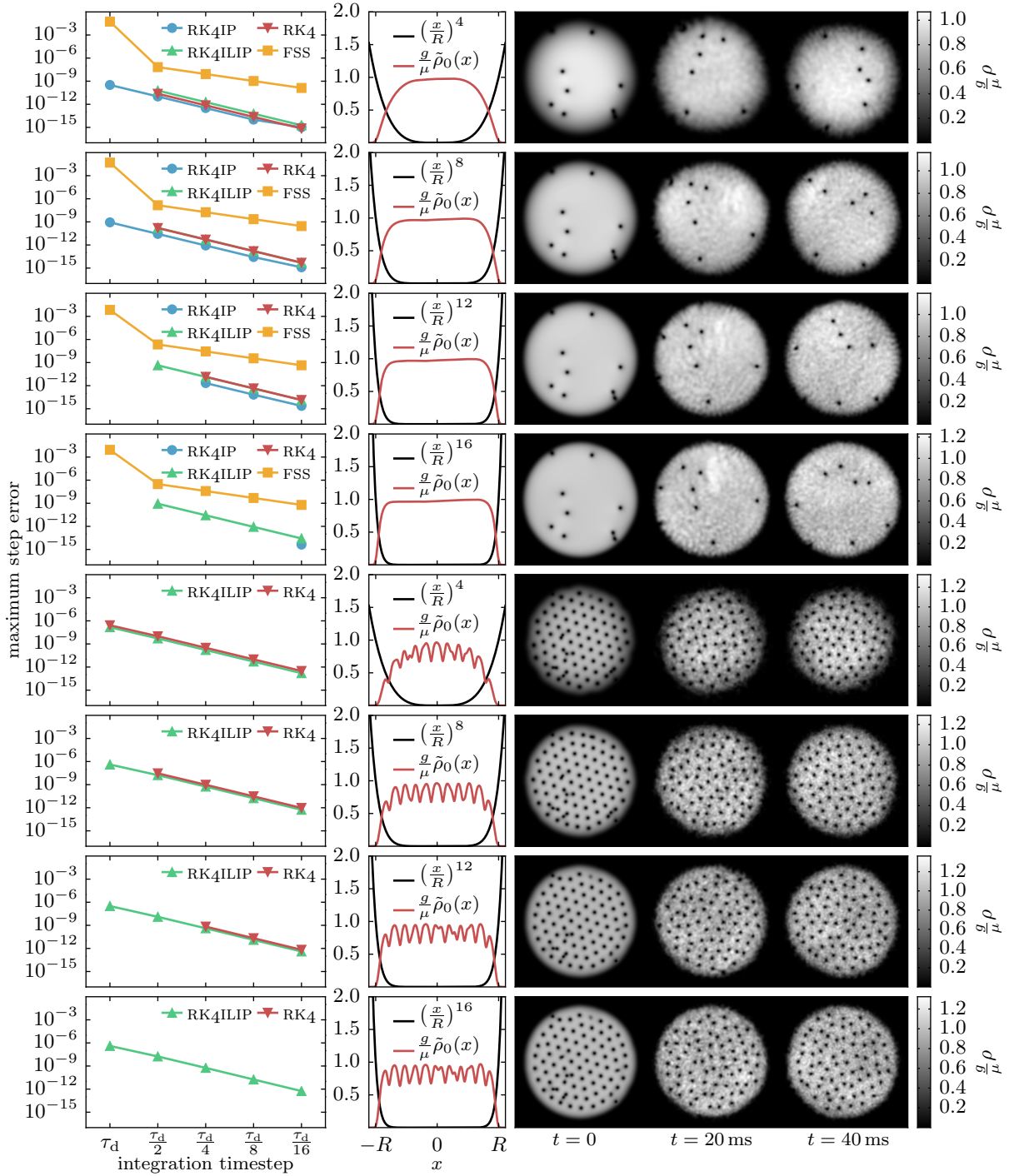


Figure 3.3: Results of simulations to compare RK4ILIP to other timestepping methods. Top four rows: Nonrotating frame simulations with four different radial power-law potentials. Bottom four rows: Rotating frame simulations with same four potentials. Left column: maximum per-step error $\int |\psi - \tilde{\psi}|^2 d\mathbf{r} / \int |\tilde{\psi}|^2 d\mathbf{r}$ of fourth order Runge–Kutta (RK4), its interaction picture variants (RK4IP and RK4ILIP) and Fourier split-step (FSS) as a function of timestep. Solutions were checked every 100 timesteps against a comparison solution $\tilde{\psi}$ computed using half sized steps for RK4 methods, and quarter sized steps for FSS. Simulations encountering numerical overflow not plotted. Centre column: potential (black) and average density $\bar{\rho}_0$ of the initial state (red) over a slice of width $R/5$ in the y direction. Right column: Density of solution at initial, intermediate and final times for each configuration simulated (taken from RK4ILIP results). RK4ILIP is the only method usable in rotating frames and not encountering overflow in the steeper traps for the timesteps considered.

rev: 45 (b37fd8d3e6c7)
author: Chris Billington
date: Fri Mar 17 17:54:14 2017 -0400
summary: Almost completed commutation error figure.

3.6.3 Results

Here I compare four numerical methods: Fourier split-step (FSS), fourth order Runge–Kutta in the interaction picture (RK4IP), ordinary fourth order Runge–Kutta (RK4), and my new method — fourth order Runge–Kutta in an instantaneous local interaction picture (RK4ILIP).

The example chosen is a 2D simulation of a turbulent Bose–Einstein condensate, in both a rotating and nonrotating frame. For the nonrotating frame the differential equation simulated was equation (3.89), and for the rotating frame the same equation was with an additional two terms added to the Hamiltonian:

$$\hat{H}_{\text{rot}} + \hat{H}_{\text{comp}} = -\boldsymbol{\Omega} \cdot \hat{\mathbf{L}} + \frac{1}{2}\hbar m^2 \Omega^2 r^2 \quad (3.92)$$

$$= i\hbar\Omega \left(x \frac{\partial}{\partial y} - y \frac{\partial}{\partial x} \right) + \frac{1}{2}\hbar m^2 \Omega^2 r^2. \quad (3.93)$$

The addition of the first term transforms the original Hamiltonian into a frame rotating at angular frequency Ω in the (x, y) plane, and is equivalent to the Coriolis and centrifugal forces that appear in rotating frames in classical mechanics [31]. The second term is a harmonic potential that exactly compensates for the centrifugal part of this force. In this way the only potential in the rotating frame is the applied trapping potential, and the only effect of the rotating frame is to add the Coriolis force.

Four trapping potentials were used, all radial power laws with different powers. These examples were chosen to demonstrate the specific situation in which RK4ILIP provides a benefit over the other methods for spatial Schrödinger-like equations, as discussed above.

The results of 120 simulation runs are shown in Figure 3.3. Each simulation was of a ^{87}Rb condensate in the $|F = 2, m_F = 2\rangle$ state, in which the two-body s -wave scattering length is $a = 98.98$ Bohr radii [32]. The simulation region was $20\text{ }\mu\text{m}$ in the x and y directions, and the Thomas–Fermi radius of the condensate was $R = 9\text{ }\mu\text{m}$. The chemical potential was $\mu = 2\pi\hbar \times 1.91\text{ kHz}$, which is equivalent to a maximum Thomas–Fermi density $\rho_{\text{max}} = 2.5 \times 10^{14}\text{ cm}^{-3}$ and a healing length $\xi = 1.1\text{ }\mu\text{m}$. There were 256 simulation grid points in each spatial dimension, which is 14 points per healing length.

Four different potentials were used, all of the form $V(r) = \mu (r/R)^\alpha$ with $\alpha = 4, 8, 12, 16$. For the rotating frame simulations, the rotation frequency was $\Omega = 2\pi \times 148\text{ Hz}$. This is 89% of the effective harmonic trap frequency, defined as the frequency of a harmonic trap that would have the same Thomas–Fermi radius given the same chemical potential.

All ground states were determined using successive over-relaxation (See section [TODO]) with sixth-order finite differences for spatial derivatives. For the nonrotating simulations, convergence was reached with $\Delta\mu/\mu < 1 \times 10^{-13}$, with:

$$\Delta\mu = \sqrt{\frac{\langle \psi | (\hat{H} - \mu)^2 | \psi \rangle}{\langle \psi | \psi \rangle}}, \quad (3.94)$$

where \hat{H} is the nonlinear Hamiltonian and $\langle \mathbf{r} | \psi \rangle$ is the condensate wavefunction, which does not have unit norm. For the rotating frame simulations the ground states converged to $\Delta\mu/\mu \approx 9 \times 10^{-7}, 2 \times 10^{-6}, 3 \times 10^{-6}$ and 2×10^{-6} for $\alpha = 16, 12, 8$, and 4 respectively.

After each ground state was found, it was multiplied by a spatially varying phase factor corresponding to the phase pattern of a number of randomly positioned vortices:

$$\psi_{\text{vortices}}(x, y) = \psi_{\text{groundstate}}(x, y) \prod_{n=1}^N e^{\pm_n i \arctan 2(y - y_n, x - x_n)} \quad (3.95)$$

where $\arctan 2$ is the two-argument arctan function,²⁶ $N = 30$, \pm_n is a randomly chosen

rev: 45 (b37fd8d3e6c7)
author: Chris Billington
date: Fri Mar 17 17:54:14 2017 -0400
summary: Almost completed commutation error figure.

sign, and (x_n, y_n) are vortex positions randomly drawn from a Gaussian distribution centred on $(0, 0)$ with standard deviation equal to the Thomas–Fermi radius R . The same seed was used for the pseudorandom number generator in each simulation run, and so the vortex positions were identical in each simulation run.

After vortex phase imprinting, the wavefunctions were evolved in imaginary time [27]. For the nonrotating frame simulations, imaginary time evolution was performed for a time interval equal to the chemical potential timescale $\tau_\mu = 2\pi\hbar/\mu$, and for the rotating frame simulations, for $\tau_\mu/10$. This was done to smooth out the condensate density in the vicinity of vortices, producing the correct density profile for vortex cores. However, since imaginary time evolution decreases the energy of the state indiscriminately, it also had the side effect of causing vortices of opposite sign to move closer together and annihilate. This decreased the number of vortices, and is the reason the smoothing step in the rotating frame simulations was cut short to $\tau_\mu/10$, as otherwise all vortices had time to annihilate with one of the lattice vortices. A vortex pair in the process of annihilating is visible in Figure 3.3 as a partially filled hole in the initial density profile near the top of the condensate in the $\alpha = 4, 12$, and 16 rotating frame simulations.²⁷

²⁷The initial states for the four different potentials are not identical, so by chance the corresponding vortex in the $\alpha = 8$ case was not close enough to a lattice vortex to annihilate.

The smoothed, vortex imprinted states were then evolved in time for 40 ms. For each simulation, five different timesteps were used: $\Delta t = \tau_d, \tau_d/2, \tau_d/4, \tau_d/8, \tau_d/16$, where $\tau_d = m\Delta x^2/\pi\hbar \approx 2.68 \mu\text{s}$ is the dispersion timescale associated with the grid spacing Δx , defined as the time taken to move one gridpoint at the phase velocity of the Nyquist mode.

For the nonrotating frame simulations, spatial derivatives for the RK4 and RK4ILIP methods were determined using the Fourier method [see section TODO]. This was to ensure a fair comparison with the other two methods, which necessarily use Fourier transforms to perform computations pertaining due to the kinetic term.

For the rotating frame simulations, sixth-order finite differences with zero boundary conditions were used instead for the kinetic terms of the RK4 and RK4ILIP methods, which were the only two methods used for those simulations (due to the other methods being incompatible with the angular momentum operator required for a rotating frame). This choice was fairly arbitrary, but did allow the condensate to be closer to the boundary than is otherwise possible with the periodic boundary conditions imposed by use of the Fourier method for spatial derivatives. This is because the rotating frame Hamiltonian is not periodic in space, and so its discontinuity at the boundary can be a problem if the wavefunction is not sufficiently small there.

As shown in Figure 3.3, all methods tested generally worked well until they didn't work at all, with the per-step error of RK4-based methods being either small and broadly the same as the other RK4-based methods, or growing rapidly to the point of numerical overflow (shown as missing datapoints). The break down of FSS was less dramatic, though it too had a clear jump in its per-step error for larger timesteps. Comparing methods therefore came down to mostly whether or not a simulation experienced numerical overflow during the time interval being simulated.

The main result was that RK4ILIP and FSS remained accurate over the widest range of timesteps and trap steepnesses, with RK4 and RK4IP requiring ever smaller timesteps in order to not overflow as the trap steepness increased.

For the rotating frame simulations, which were only amenable to the RK4 and RK4ILIP methods, the same pattern was observed, with RK4 only working at smaller timesteps as the trap steepness was increased, and ultimately diverging for all timesteps tested at the maximum trap steepness. By contrast, RK4ILIP remained accurate over the entire range of timesteps at the maximum trap steepness.

3.6.4 Discussion

²⁸This is essentially due to such a situation violating the condition we laid out at the beginning of this section — that the simulation basis must be nearly an eigenbasis of the total Hamiltonian.

As mentioned, RK4ILIP is mostly useful for continuum quantum mechanics only when there are large spatial differences in the potential, which cannot give rise to equally large kinetic energies²⁸. Furthermore, the advantage that RK4ILIP has over other methods with that same property is that it does not require a particular form of Hamiltonian or a particular method of evaluating spatial derivatives. The former means it is applicable in rotating frames or to situations with unusual Hamiltonians, and the latter means it can be used with finite differences or FEDVR [21] and thus is amenable to parallelisation on a cluster computer.

The ability to model large spatial variations in the potential provides only a narrow domain of increased usefulness over other methods. If a large kinetic energy results from the large potential, then the method requires just as small timesteps as any other. And if the large potential is supposed to approximate an infinite well, then an actual infinite well may be modelled using zero boundary conditions, negating the need for something like RK4ILIP. However, when potential wells are steep, but not infinitely steep, here RK4ILIP provides a benefit. The only other model that can handle these large potentials—Fourier split-step—has the disadvantage that it cannot deal with arbitrary operators such as those arising from a rotating frame, and is not parallelisable with local data. The benefits of parallelisability are obvious, and the above results demonstrate RK4ILIP's advantage at simulating BECs in tight traps and rotating frames.

Note that whilst the *Fourier* split-step method can't handle Hamiltonian terms such as $\hat{r} \cdot \hat{p}$ that are not diagonal in either real space or Fourier space [14, p315], a split-step method based on an approximation to the momentum operator as a banded matrix, such as that obtained with finite differences, can. Using the techniques discussed in section 3.2.3, such a scheme is also parallelisable. The remaining limitations then, when compared to fourth-order Runge–Kutta are the restriction on the types of nonlinearity that can be included, and the complexity of implementation.

For systems with discrete degrees of freedom, RK4ILIP may be useful in the case where an approximate diagonalisation of the Hamiltonian is analytically known, and when the Hamiltonian's eigenvalues vary considerably in time (making a single interaction picture insufficient to factor out dynamical phases throughout the entire simulation). In this situation an analytic transformation into the diagonal basis can be performed at each timestep (or the differential equation analytically re-cast in that basis in the first place), and RK4ILIP can be used to factor out the time-varying dynamical phase evolution at each timestep. An example may be an atom with a magnetic moment in a time-varying magnetic field which varies over orders of magnitude. The transformation into the spin basis in the direction of the magnetic field can be analytically performed, and if the field varies by orders of magnitude, so do the eigenvalues of the Hamiltonian. Although the eigenvalues in this case and other similar cases can be computed analytically too, unless all time dependence of the Hamiltonian is known in advance of the simulation, it would be difficult to incorporate this into a re-casting of the differential equation in a time-dependent interaction picture. RK4ILIP may be useful in these cases to automate this process and evolve the system in the appropriate interaction picture at each timestep.

rev: 45 (b37fd8d3e6c7)
 author: Chris Billington
 date: Fri Mar 17 17:54:14 2017 -0400
 summary: Almost completed commutation error figure.

z

rev: 45 (b37fd8d3e6c7)
author: Chris Billington
date: Fri Mar 17 17:54:14 2017 -0400
summary: Almost completed commutation error figure.

This page intentionally left blank

References

- [1] L. M. Bennie, P. B. Wigley, S. S. Szigeti, M. Jasperse, J. J. Hope, L. D. Turner, and R. P. Anderson. *Precise wavefunction engineering with magnetic resonance*. arXiv:1412.6854 (2014). ARXIV: [1412.6854](#). [p 1]
- [2] A. Görlitz, J. M. Vogels, A. E. Leanhardt, C. Raman, T. L. Gustavson, J. R. Abo-Shaeer, A. P. Chikkatur, S. Gupta, S. Inouye, T. Rosenband, and W. Ketterle. *Realization of Bose-Einstein Condensates in Lower Dimensions*. Physical Review Letters **87**, 130402 (2001). DOI: [10.1103/PhysRevLett.87.130402](#). [p 2]
- [3] S. Hofferberth, I. Lesanovsky, B. Fischer, T. Schumm, and J. Schmiedmayer. *Non-equilibrium coherence dynamics in one-dimensional Bose gases*. Nature **449**, 324 (2007). DOI: [10.1038/nature06149](#). [p 2]
- [4] B. Rauer, P. Grišins, E. Mazets, I. T. Schweigler, W. Rohringer, R. Geiger, T. Langen, and J. Schmiedmayer. *Cooling of a one-dimensional Bose gas*. Physical Review Letters **116**, 030402 (2016). DOI: [10.1103/PhysRevLett.116.030402](#). [p 2]
- [5] P. D. Lett, R. N. Watts, C. I. Westbrook, W. D. Phillips, P. L. Gould, and H. J. Metcalf. *Observation of Atoms Laser Cooled below the Doppler Limit*. Physical Review Letters **61**, 169 (1988). DOI: [10.1103/PhysRevLett.61.169](#). [p 2]
- [6] J. Dalibard and C. Cohen-Tannoudji. *Laser cooling below the Doppler limit by polarization gradients: Simple theoretical models*. JOSA B **6**, 2023 (1989). DOI: [10.1364/JOSAB.6.002023](#). [p 2]
- [7] M. Saffman, T. G. Walker, and K. Mølmer. *Quantum information with Rydberg atoms*. Reviews of Modern Physics **82**, 2313 (2010). DOI: [10.1103/RevModPhys.82.2313](#). [p 2]
- [8] E. Urban, T. A. Johnson, T. Henage, L. Isenhower, D. D. Yavuz, T. G. Walker, and M. Saffman. *Observation of Rydberg blockade between two atoms*. Nature Physics **5**, 110 (2009). DOI: [10.1038/nphys1178](#). [p 2]
- [9] B. B. Blinov, J. R. N. Kohn, M. J. Madsen, P. Maunz, D. L. Moehring, and C. Monroe. *Broadband laser cooling of trapped atoms with ultrafast pulses*. JOSA B **23**, 1170 (2006). DOI: [10.1364/JOSAB.23.001170](#). [p 2]
- [10] A. J. McCulloch, D. V. Sheludko, M. Junker, and R. E. Scholten. *High-coherence picosecond electron bunches from cold atoms*. Nature Communications **4**, 1692 (2013). DOI: [10.1038/ncomms2699](#). [p 2]

rev: 45 (b37fd8d3e6c7)
author: Chris Billington
date: Fri Mar 17 17:54:14 2017 -0400
summary: Almost completed commutation error figure.

- [11] T. Brabec and F. Krausz. *Intense few-cycle laser fields: Frontiers of nonlinear optics*. Reviews of Modern Physics **72**, 545 (2000). DOI: [10.1103/RevModPhys.72.545](https://doi.org/10.1103/RevModPhys.72.545). [p 2]
- [12] C. Brezinski. *Extrapolation algorithms and Padé approximations: A historical survey*. Applied Numerical Mathematics **20**, 299 (1996). DOI: [10.1016/0168-9274\(95\)00110-7](https://doi.org/10.1016/0168-9274(95)00110-7). [p 4]
- [13] C. Moler and C. Van Loan. *Nineteen Dubious Ways to Compute the Exponential of a Matrix, Twenty-Five Years Later*. SIAM Review **45**, 3 (2003). DOI: [10.1137/S00361445024180](https://doi.org/10.1137/S00361445024180). [p 4]
- [14] D. J. Tannor. *Introduction to Quantum Mechanics: A Time-Dependent Perspective*. University Science Books (2007). [pp 5, 9, and 32]
- [15] S. Weinzierl. *Introduction to Monte Carlo methods*. arXiv:hep-ph/0006269 (2000). ARXIV: [hep-ph/0006269](https://arxiv.org/abs/hep-ph/0006269). [p 6]
- [16] F. J. Dyson. *The S Matrix in Quantum Electrodynamics*. Physical Review **75**, 1736 (1949). DOI: [10.1103/PhysRev.75.1736](https://doi.org/10.1103/PhysRev.75.1736). [p 6]
- [17] V. Kaplunovsky. On Perturbation Theory, Dyson Series, and Feynman Diagrams. <http://bolvan.ph.utexas.edu/~vadim/Classes/2016f/dyson.pdf>, (2016). Online lecture notes. [p 6]
- [18] M. Suzuki. *Quantum Monte Carlo Methods in Condensed Matter Physics*. World Scientific (1993). [p 10]
- [19] B. I. Schneider and L. A. Collins. *The discrete variable method for the solution of the time-dependent Schrödinger equation*. Journal of Non-Crystalline Solids **351**, 1551 (2005). DOI: [10.1016/j.jnoncrysol.2005.03.028](https://doi.org/10.1016/j.jnoncrysol.2005.03.028). [p 10]
- [20] M. Suzuki. *General Decomposition Theory of Ordered Exponentials*. Proceedings of the Japan Academy, Series B **69**, 161 (1993). DOI: [10.2183/pjab.69.161](https://doi.org/10.2183/pjab.69.161). [p 10]
- [21] B. I. Schneider, L. A. Collins, and S. X. Hu. *Parallel solver for the time-dependent linear and nonlinear Schrödinger equation*. Physical Review E **73**, 036708 (2006). DOI: [10.1103/PhysRevE.73.036708](https://doi.org/10.1103/PhysRevE.73.036708). [pp 14, 27, and 32]
- [22] J. Javanainen and J. Ruostekoski. *Symbolic calculation in development of algorithms: Split-step methods for the Gross–Pitaevskii equation*. Journal of Physics A: Mathematical and General **39**, L179 (2006). DOI: [10.1088/0305-4470/39/12/L02](https://doi.org/10.1088/0305-4470/39/12/L02). [p 16]
- [23] J. J. Sakurai. *Modern quantum mechanics*. Addison-Wesley Pub. Co, Reading, Mass (1994). [p 23]
- [24] B. M. C. Davies. *Vortex dynamics in Bose–Einstein condensates*. PhD thesis, University of Otago, Dunedin, New Zealand (2000). [p 25]
- [25] W. Press. *The art of scientific computing*. Cambridge University Press (1992). [p 25]
- [26] C. Pethick and H. Smith. *Bose–Einstein condensation in dilute gases*. Cambridge University Press (2002). [p 25]
- [27] M. L. Chiofalo, S. Succi, and M. P. Tosi. *Ground state of trapped interacting Bose–Einstein condensates by an explicit imaginary-time algorithm*. Phys. Rev. E **62**, 7438 (2000). DOI: [10.1103/PhysRevE.62.7438](https://doi.org/10.1103/PhysRevE.62.7438). [pp 26 and 31]

rev: 45 (b37fd8d3e6c7)

author: Chris Billington

date: Fri Mar 17 17:54:14 2017 -0400

summary: Almost completed commutation error figure.

- [28] G. M. Muslu and H. A. Erbay. *Higher-order split-step Fourier schemes for the generalized nonlinear Schrödinger equation*. Mathematics and Computers in Simulation **7**, 581 (2005). DOI: [10.1016/j.matcom.2004.08.002](https://doi.org/10.1016/j.matcom.2004.08.002). [p 27]
- [29] M. Heroux, P. Raghavan, and H. Simon. *Parallel processing for scientific computing*. Society for Industrial and Applied Mathematics, Philadelphia, PA (2006). [p 27]
- [30] A. Gupta and V. Kumar. *The scalability of FFT on parallel computers*. IEEE Transactions on Parallel and Distributed Systems **4**, 922 (1993). [p 27]
- [31] P. Gulshani and D. J. Rowe. *Quantum mechanics in rotating frames. I. The impossibility of rigid flow*. Canadian Journal of Physics **56**, 468 (1978). DOI: [10.1139/p78-060](https://doi.org/10.1139/p78-060). [p 30]
- [32] E. G. M. van Kempen, S. J. J. M. F. Kokkelmans, D. J. Heinzen, and B. J. Verhaar. *Interisotope determination of ultracold rubidium interactions from three high-precision experiments*. Phys. Rev. Lett. **88**, 093201 (2002). DOI: [10.1103/PhysRevLett.88.093201](https://doi.org/10.1103/PhysRevLett.88.093201). [p 30]

rev: 45 (b37fd8d3e6c7)
author: Chris Billington
date: Fri Mar 17 17:54:14 2017 -0400
summary: Almost completed commutation error figure.

This page intentionally left blank

Word count

Total

Words in text: 25704

Words in headers: 278

Words outside text (captions, etc.): 3819

Number of headers: 68

Number of floats/tables/figures: 28

Number of math inlines: 623

Number of math displayed: 109

Files: 9

Subcounts:

text+headers+captions (#headers/#floats/#inlines/#displayed)

1753+28+325 (9/2/26/8) File(s) total: atomic_physics.tex

725+17+385 (4/4/7/0) File(s) total: experiment.tex

50+0+0 (0/0/0/0) File(s) total: front_matter.tex

1370+19+65 (3/2/39/13) File(s) total: hidden_variables.tex

2043+7+145 (3/1/4/0) File(s) total: introduction.tex

12575+139+1449 (28/4/469/84) File(s) total: numerics.tex

4435+33+760 (11/9/1/0) File(s) total: software.tex

2717+22+690 (7/6/77/4) File(s) total: velocimetry.tex

36+13+0 (3/0/0/0) File(s) total: wave_mixing.tex

rev: 45 (b37fd8d3e6c7)

author: Chris Billington

date: Fri Mar 17 17:54:14 2017 -0400

summary: Almost completed commutation error figure.